2014

Synthesis, X-Ray Crystallography, And Spectroscopic Studies Of Lanthanide Complexes Nitrogen Of Donor Ligand

Jennifer Laverne Stanley
North Carolina Agricultural and Technical State University

Synthesis, X-ray Crystallography, and Spectroscopic Studies of Lanthanide Complexes Nitrogen of Donor Ligand

Jennifer Laverne Stanley

North Carolina A&T State University

A thesis submitted to the graduate faculty

in partial fulfillment of the requirements for the degree of

MASTER OF SCIENCE

Department: Chemistry

Major: Chemistry

Major Professor: Dr. Zerihun Assefa

Greensboro, North Carolina

2014

The Graduate School
North Carolina Agricultural and Technical State University

This is to certify that the Master's Thesis of

Jennifer Laverne Stanley

has met the thesis requirements of
North Carolina Agricultural and Technical State University

Greensboro, North Carolina
2014

Approved by:

Dr. Zerihun Assefa Major Professor	Dr. Sayo Fakayode Committee Member
Dr. Margaret Kanipes-Spinks Department Chair	Dr. Julius Harp Committee Member

Dr. Sanjiv Sarin
Dean, The Graduate School

Biographical Sketch

Jennifer Laverne Stanley was born on March 7, 1987, in Atlanta Georgia. She graduated from East Laurens High School in 2005. She received the Bachelor of Science degree in Chemistry from Savannah State University in 2010. In the fall 2012 she was accepted to North Carolina Agricultural and Technical State University to obtain her Masters of Science degree in Chemistry.

Dedication

This thesis is dedicated to my wonderful mother Annie Stanley, my dad and step dad Johnny Mitchell and Tyrus Stanley Sr., my grandparents Mr. and Mrs. Johnson, and my brothers and sisters Devon Mitchell, Jermane Stanley, Tyrus Stanley, Zachary Whipple, Steven Whipple, Tyressa Stanley and Tanya Malloy (Pinder). I would also like to dedicate my thesis to my cousin/aunt Francenia Whipple and her husband Steven Whipple.

Acknowledgments

First giving honor to God, who has been there when no one else was and given me the wisdom, knowledge and understanding to get me through this process. Deep appreciation goes to my mother and siblings who believes in me more than I do sometimes. Sincere gratitude goes to my advisor Dr. Assefa who has trained me to become an independent researcher and has helped me build confidence within myself. To my committee Dr. Harp and Dr. Fakayode, thank you. A special appreciation goes to Darkus who has showed me tough love and has helped me in more ways than I can ever return the favor. She has showed me that it is true that you can get anywhere from SSU. I am also thankful for Dr. Pinder who has helped me in more ways than could ever be imagined. I have to acknowledge my group members who have been there to keep me on track and have helped me from the beginning to the end. Thank you to the Department of Chemistry (NCAT) faculty, staff and students.

Table of Contents

List of Figures

List of Tables

Nomenclature

ED	Electric Dipole
EtOH	Ethanol
MD	magnetic Dipole
MeOH	Methanol
MeCN	Acetonitrile
mL	Milliliter
g	Gram
nm	Nanometer
min	Minutes
TPAO	1, 3, 5-triaza-7-phosophaadamantane-7-oxide
Phen	5-Nitro-1, 10-Phenanthroline
Terpy	4’-(4-methylyphenyl)-2, 2’:6’, 2”-terpyridine
Ln	Lanthanide
IR	Infrared Spectroscopy

Abstract

In this study, several new compounds containing N-based donor ligands and group 11 transitions metal complexes were prepared and studied through luminescence, infrared, Raman, and other spectroscopic techniques. The coordinating N containing ligands used in this study were terpyridine (terpy) and phenanthroline (phen) derivatives, and TPAO (triazaphosphaadamantane oxide). TPAO was used to substitute some of the H_2O quencher and to probe whether it could also act as an effective sensitizer. The photoluminescence studies show characteristic f-f emissions of the Tb^{3+} and Eu^{3+} ions. For the Tb^{3+} complexes the strongest band (hypersensitive band) was observed ~ 540nm corresponding to the $^5D_4 \rightarrow {}^7F_5$ transition, while for Eu^{3+} complexes the band at 615nm corresponding to the $^5D_0 \rightarrow {}^7F_2$ transition dominates. The excitation spectra in both systems provides a strong band at ~358 nm corresponding to $\pi - \pi^*$ transition the terpy ligand and ~380nm for $Au(CN)_2^-$. Terpy with phenanthroline derivatives were also explored which yielded four new compounds – $[Tb(H_2O)_4(Au(CN)_2)(C_{22}H_{17}N_3)(TPAO)]Cl_3$ **(1)** ,$[Eu(H_2O)_4(Au(CN)_2)(C_{22}H_{17}N_3)]Cl_3$ **(2)**, $[Tb(H_2O)_4(Au(CN)_2)(C_{22}H_{17}N_3)]Cl_3$ **(3)** and $[Eu(H_2O)_4Au(CN)_2(Phen)]Cl_3$ **(4)**. New understanding regarding the mode of interaction is reported as well as spectroscopic data of these complexes.

CHAPTER 1

Introduction

1.1 Luminescence

Luminescence was first discovered by Sir G. G. Stokes in 1852 [1]. Luminescence is also one of the most sensitive spectroscopic techniques that are used today. It comes from the root (Lume=light), which can be defined as a spontaneous emission of radiation from an electronically or vibrationally excited species [2]. To classify all forms of light that are not solely conditioned by the rise of temperature, Eilhardt Wiedeman introduced the term "luminescenz"[1-2]. Due to the modes of excitation luminescence can be separated into different categories. These categories are: chemiluminescence (is the phenomenon in which a chemical reaction leads to the emission of light without incandescence), bioluminescence (emission of visible light by living organisms), electroluminescence (emission of light caused by electric discharge in a gas), cathodoluminescence (luminescence caused by irradiation with electrons), radioluminescence (luminescence that is induced by radiation from a radioactive material), thermoluminescence (phosphorescence produced by the heating of a substance), and photoluminescence (emission of light that occurs form direct photoexcitation of the emitting species). Photoluminescence is one of our main research goals. [3]

Photoluminescence has two well-known forms which are fluorescence and phosphorescence. Fluorescence is the radiative decaying from the exciting state to the ground state of the same multiplicity, which makes these types of transitions 'allowed" [4]. The emissive rate for fluorescence is usually near 10^8 per seconds [5]. The lifetime for fluorescence is 10^{-8} per seconds, since the emissive rate is relatively fast it causes the lifetime to very low [5]. The lifetime determines the average time a fluorophore remains in the excited state [6]. The second

type of photoluminescence is phosphorescence, which is the radiative decaying from the exciting state to a ground state with different multiplicity [5]. These types of transitions are not allowed. The emissive rate for phosphorescence is very slow, which makes the lifetime relative fast. The lifetime for the phosphorescence ranges from milliseconds to seconds, depending solely on deactivation process[2].

In the 19th century G. G. Stokes identified the difference between fluorescence and phosphorescence by the duration of emission after excitation of the species [2]. Later studies showed that G.G. Stokes criterion were insufficient because there are long-lived fluorescence and short-lived phosphorescence [2]. However, in 1929 Francis Perrin identified the difference between fluorescence and phosphorescence by spin multiplicity. For fluorescence spin multiplicity is retained $^1S_1 \rightarrow {}^1S_0$, whereas phosphorescence involves a change in spin multiplicity $^1S_1 \rightarrow {}^3T_1$ (shown in figure 1.1)[2] .

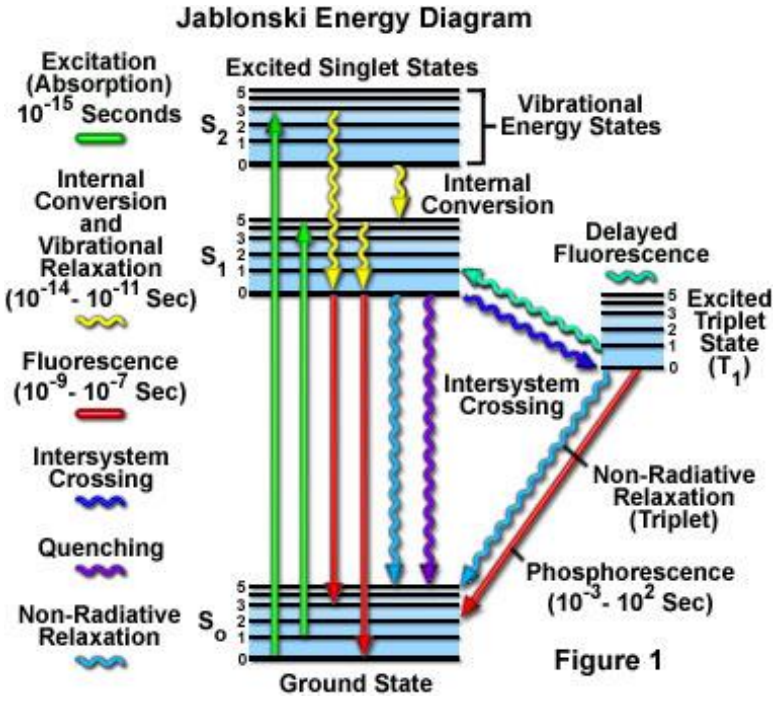

Figure 1.1. Jablonski Energy Diagram

Photoluminescent complexes are those that emit radiation after it has been electronically excited. These complexes also deal with nonradiative decaying[7]. Luminescence from lanthanide (III) ions is the result of completion between radiative and non –radiative pathways in the relaxation of an electronically excited species [7]. "The multitude of electronic energy level due to the f electrons allows for a rich cascade of radiative and non –radiative relation processes in excited lanthanide ions" [7].

Radiative transitions in the free lanthanide ions theoretically only allow magnetic dipole (MD) transitions to be allowed [7]. This is done by the change in the total angular momentum (ΔJ) of the electrons. Europium (III) emission at ~590 nm is an example of a MD transition. However, radiative transitions differ when placed into a coordination environment. When coordination takes place electric dipole (ED) transitions are induced as ligand field mixing odd-parity configuration slight in the $4f^n$ to $5d^0$ configurations [7]. There are transitions that acquire both MD and ED contributions. For example, terbium (III) emission spectrum is dominated by both MD and ED transitions [7]. MD and induced ED transitions of lanthanide ions are weak when compared to transitions that are fully allowed.

Non-radiative deactivation in luminescent lanthanide complexes is as important as radiative luminescence. This process of molecular high-energy vibration in organic ligands and solvents makes non-radiative relation of excited lanthanide ions much more efficient [7]. The aim when developing luminescent lanthanide complexes are to protect the ion from quenches, such as O-H vibrations of water, which are good quenchers of lanthanide luminescence [7]. Tb(III) and Eu (III) complexes prevent a real challenge for non-radiative deactivation in complexes near-

infrared luminescent ions that are intrinsically more sensitive to quenching by molecular vibrations [7].

1.2 Lanthanides

Scandinavia is the birth place for lanthanide chemistry[8]. Gadolinite also known as earth yttria was discovered in 1794 by Johann Gadoline [8]. However, in the early 1840s Swede C. G. Mosander separated earth into their component oxides, which we know as cerium and lanthanum today[8]. Henry Moseley was the first to analysis different lanthanides using X-ray in 1907[8]. He also showed that there were 14 lanthanides ranging from Lanthanum (atomic number 57) to Lutetium (atomic number 71), which are all electropositive[5, 8-9]. These lanthanides are known as "rare earth metals".

These rare earth metals exhibits numerous features, which differentiate them from the d-block metals. Lanthanides coordination number ranges from six to twelve[8]. For Terbium and Europium which is used in our research group the coordination number could be eight or nine. Ligand steric determines coordination geometries rather than the crystal field effects[8]. Lanthanides have small crystal-field splitting and very sharp electronic spectra[8]. Lanthanide favors the +3 oxidation state. Since the 4f orbitals are well shielded by the $5s^2$ and $5p^6$ orbitals they do not participate directly in bonding, and this makes spectroscopic and magnetic properties uninfluenced by ligands[8]. "They form labile 'ionic' complexes that undergo facile exchange of ligand"[8]. These Ln^{3+} ions do not extend past the xenon core, because there is no longer s and d electrons[5] . Ln^{3+} ions are hard Lewis acids that have high affinity to hard bases, such as oxygen and nitrogen. Electronic spectra of lanthanide systems have a variety of colors, [1]. Lanthanides actual absorption bands are associated with f-f electronic transitions which are Lapporte forbidden transitions [1]. These f-f transitions have large numbers of weak and sharp bands. The

absorption bands of these transitions are closely related to the emission spectrum corresponding to the ion [1]. In addition there are also electron-transfer bands, which have broad, intense bands that are found in the UV region for selected lanthanide systems including, cerium, samarium and europium ions [1] .

When considering coordination of all trivalent lanthanides ligand, it occurs predominantly via ionic bonding interactions. The ionic bonding interactions of trivalent lanthanides leads to a strong preference for negatively charged donor groups (hard bases). Trivalent lanthanides prefer coordinating to water molecules and hydroxide ions, so while in aqueous solution ligands with negatively charged oxygen will bind strongly. Even though Ln^{3+} prefer ligands donors groups that have negative charged oxygen they will also bind to ligands with neutral donors such as nitrogen and oxygen. However in order for Ln^{3+} to bind to ligands with neutral donor site it must have donor site that is a hard base.

Coordination of lanthanides electric dipole transitions are favored as the ligand field mixes odd parity configurations. Coordinating chromophores absorb energy, several lines of absorption and emission is due to electric dipole transition [3a]. Both magnetic dipole and electric dipole transitions of lanthanide ions are weak compared to fully allowed transition in organic chromophores [3a] . Lanthanides excited state is relaxed by radiative process and non-radiative process. Organic chromophores have high energy vibrations. Because of organic chromophores the excitation energy of lanthanide complexes can be dissipated by vibrations of surrounding matrix through a process known as multi-phonon relaxation[3a] . The efficiently in lanthanides undergo multi-phonon relation, which is due to low energy gap that cause immediate decay to take place from the higher excited state to low lying excited state [3a].

1.2.1 Terbium. Carl Gustaf Mosander was the first to discover and first isolate terbium in the mid-1800s. Terbium (Tb) is a block F, group 3, period 6 element. Terbium atom has a Van der Waals radius of 221 ppm and radius of 177 pm [10]. Tb (III) is a hard acid and has a coordination number of nine. Tb (III) interacts great with hard bases such as oxygen. Even though Tb (III) prefers harder bases they will also react with nitrogen which is a softer base. Terbium also forms stable chelates with negative charged donating ligands. Terbium shows intense emission bands at 490, 545, and 590 nm, corresponding to $^5D_4 \rightarrow {}^7F_6$, $^5D_4 \rightarrow {}^7F_5$, $^5D_4 \rightarrow {}^7F_4$, and $^5D_4 \rightarrow {}^7F_3$ transitions, respectively. The emission band of Tb^{3+} at 545nm is the most sensitive, as shown in figure 1.2. Terbium is used in green phosphors in fluorescent lamps and color TV tubes.

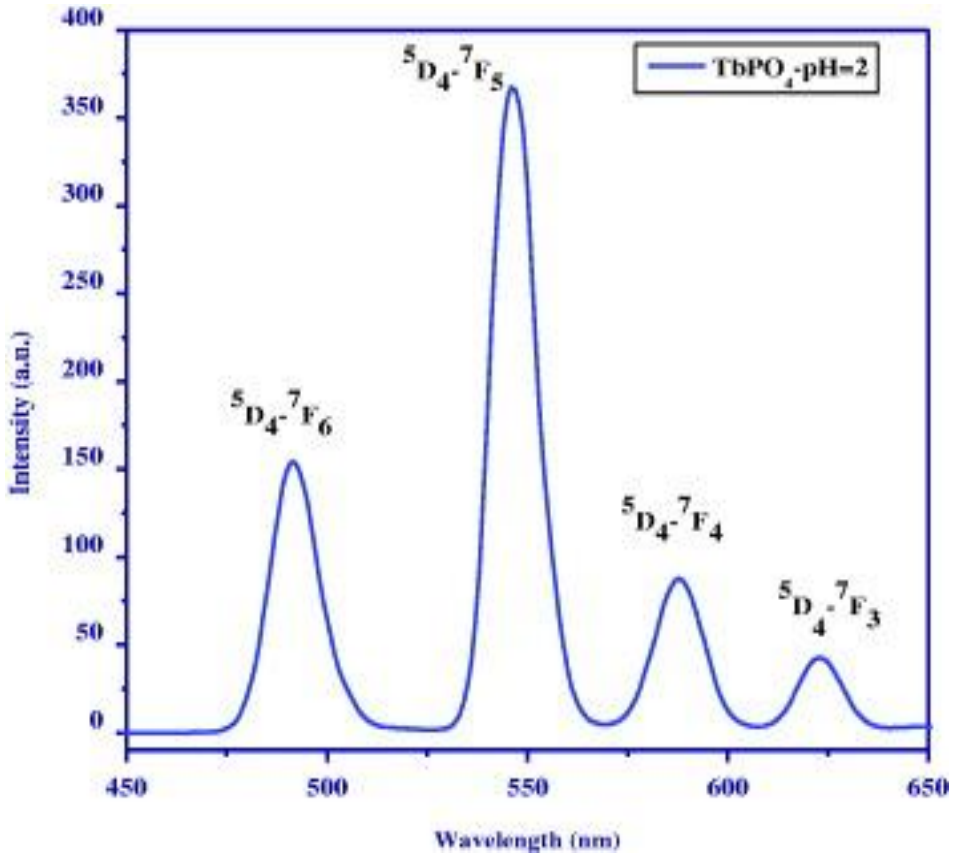

Figure 1.2. Emission spectrum of terbium (III)

1.2.2 Europium. Europium (Eu) is a chemical element found in the lanthanide series with an atomic number of 65. Europium is named after Europe. It is rare earth metal that is silvery white soft metal. In the lanthanide series europium is the softest and least dense. It also is very easy to oxidize in the air. Europium is a ductile metal that crystallizes in a body-centered cubic lattice [4]. The most common oxidation state of europium is +3. Europium (III) generally has a coordination number of eight or nine. Europium properties are influenced by its half-filled electron shell**.** Eu^{3+} ions have relatively large energy gap between the lowest emission level and the ground state[10] . Europium (III) has emission bands at 580, 590, 613, 650, 690, and 710nm corresponding to the $^5D_0 \rightarrow {}^7F_0$, $^5D \rightarrow {}^7F_1$, $^5D_0 \rightarrow {}^7F_2$, $^5D_0 \rightarrow {}^7F_3$, $^5D_0 \rightarrow {}^7F_4$, and $^5D_0 \rightarrow {}^7F_5$ transitions, respectively. Eu (III) most intense band is at 613nm. However, at 580nm ($^5D_0 \rightarrow {}^7F_0$) the transition is a forbidden transition and is weak. This transition is prohibited due to the selection rules[11] .

1.3 Energy Transfer

There has been a wide range of studies/observations on emission for lanthanide ions under various conditions. Since Lanthanide ions have very intense luminescent properties and have long luminescent lifetimes and line-like emission they are used as phosphors and lasers[12]. A great number of lanthanide ion exhibits materials containing lanthanide ions have been used as phosphors and laser materials because of their sharp, intensely luminescent f-f electronic transitions. In particular, a number of lanthanide complexes display a bright and narrow emission lines. Because lanthanide ion have low extinction coefficient it makes direct photoexcitation difficult. This can be overcome by using energy transfer process from organic chromophores to lanthanide ions.

The lanthanide ions Eu(III), and Tb(III) have large energy gap between lowest luminescent excited states to highest ground state manifold[12b, 13]. Hence these ions show strong visible luminescence because of the reduced vibrational quenching that could bridge the gap of non-radiative pathway. The luminescence intensity and excited state lifetime is linearly proportional to the number of quenchers present inside the inner coordination sphere of lanthanide ion[14]. Quenching can be overcome by incorporating chromophores. Chromophores generally help remove solvent and water molecule from the inner coordination sphere of the lanthanide ions**.** Hence, chromophores assist in the enhancing luminescence of lanthanides [9]. Chromophores also provides alternate pathway for energy transfer and they enlarge the Stokes shift[9].

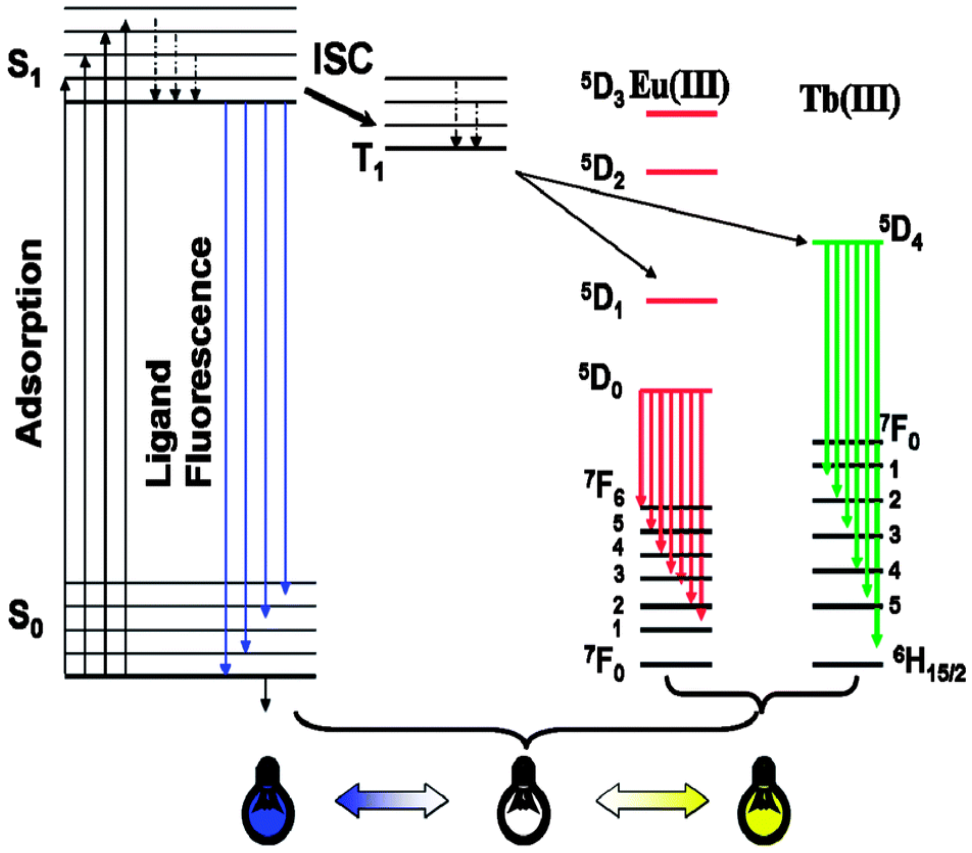

Figure 1.3. Energy transfer diagram of luminescent lanthanide complexes

1.4 Ligands

Ligands are molecules or ions that bind to a central atom to form a complex molecule. They are either neutral or negatively charged molecules, and are usually known as electron donors or bases, whereas the metal functions as the Lewis acid or electron acceptor. Ligands provided the electron for the bond to the central metal, which in this case Tb^{3+} or Eu^{3+}. The ligands that are being proposed in this research have nitrogen binding sites. There has been several synthesis using nitrogen donor ligands, such as terpyridine ligands. These terpyridine ligands are used to form complexes with different lanthanides, such as Tb^{3+} and Eu^{3+}. These lanthanides are used because of their luminescent properties, and because they are enhanced by the absorbent chelating ligands.

Organic ligands are currently used in research to help enhance the luminescence because they are efficient sensitizers for the luminescence of Ln (III) ions, meaning that Ln (III) ions have a low molar absorption coefficient[15]. Coordinating Ln (III) ions to organic ligands (polydentate ligand) with multiple binding sites helps to change the overall symmetry of the complexes as well as decreases the coordination number of Ln (III) ions. In addition to polydentate ligands reducing coordination site to Ln (III) ions, decrease the non-radiative energy loss therefore, increase luminescence[16]. Figure 1.4 shows how chromophore (organic ligands) operates as an antenna, absorbing light then transferring this excitation to the metal ion, which can then deactivate by undergoing its typical luminescent emission [6-7]. The usual impediment in lanthanide ion systems is that direct absorption of the f-f excited states is very inefficient. Hence, a light harvesting ligand is essential to enhance the emission from the metal cation site. Donor ligands used for such applications usually have strong absorbance in the UV region and transfer their excited energy to the acceptor lanthanide ions.

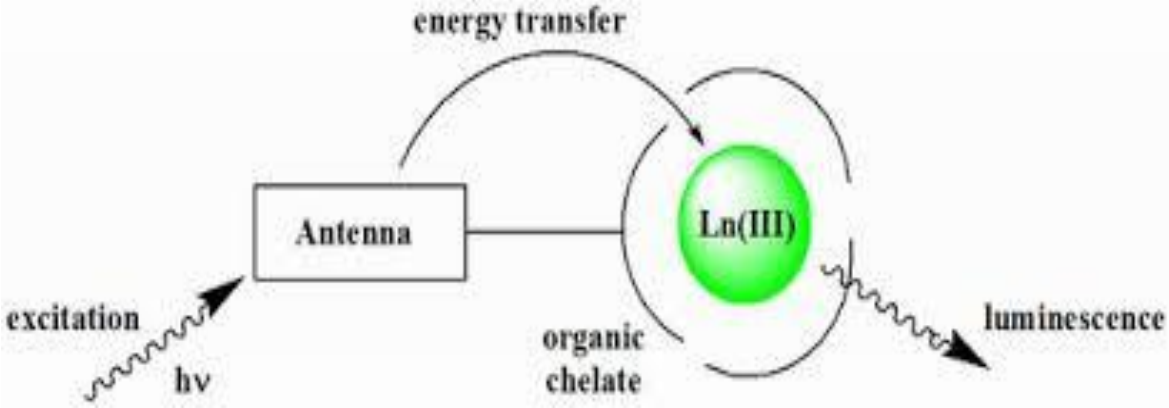

Figure 1.4. Energy transfer when chomophores act as an antenna

1.4.1 Terpyridine Ligands. Terpyridines (also known as terpy) are N-donor ligand that contains three nitrogen donor binding sites, which is consider as a tridentate ligand. This asymmetric tridentate ligands 4'-(4-methylphenyl)-2 2' 6' 2"-terpyridine, is used in this research because of its high binding affinity to form complexes with ternary rare earth metals, which have very intense emission[17]. This N-heterocyclic ligand features makes it useful in ability to absorb excitation near-UV radiations and channel it to the Ln(III) ions[15]. Since the terpy ligand is a donor system that absorbs in the UV region and has been shown to undergo energy transfer processes with select lanthanide cation; a number of compounds have been reported to contain terpy, or derivatives thereof that act as light harvesting antenna and can subsequently transfer absorbed energy to coordinated Ln^{3+} cations. One of our research aims is to prepare compounds that contain multiple donor species that can cooperatively enhance the lanthanide emission. In doing so we hope to (1) broaden the energy range for donor light harvesting and (2) create systems with highly efficient lanthanide luminescence via cooperative energy transfer from the donor groups. In this study we used a combination of an organic ligand and group 11 transition metal complexes as dual sensitizers of the lanthanide emission.

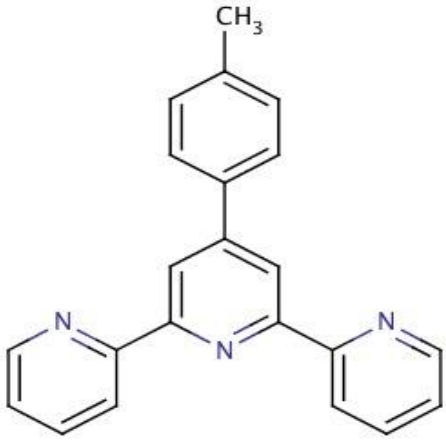

Figure 1.5. 4'-(4-methylphenyl)-2 2' 6' 2"-terpyridine

1.4.2 Phenanthroline Ligands. Phenanthroline is an N-donor ligand with two nitrogen donor binding sites. This bidentate ligand plays an important role in lanthanide complexes. "Phenanthroline is a rigid planar, hydrophobic, electron poor heteroaromatic system whose nitrogen atoms are beautifully placed to act cooperatively in cation binding" [16-18]. In aqueous solution phenanathroline act as a weak base, and also form octahedral complexes with first row transition metals [18]. Since phenanthroline is basic it attracts Ln (III) ions increasing its binding affinity to form complexes. Octahedral complexes have been study such as $[M(phen)]^{2+}$, ($[Mn(phen)]^{2+}$), and ($[Cu(phen)]^{2+}$) which are very stable complexes and exhibit great entropic contribution due to the hydrophobic nature[16, 18-19].

5-Nitro-1, 10-phenanthroline is a phenanthroline derivative that is used in this researcher shown in Figure 1.5. This derivative is bidentate ligands due to the two nitrogen donor sites that can bind to metals such as Tb^{3+} and Eu^{3+}. However, since phenanthroline is hydrophobic solubility in water seems unlikely. However, phenanthroline is slightly soluble in water, and very soluble in other polar solvents.

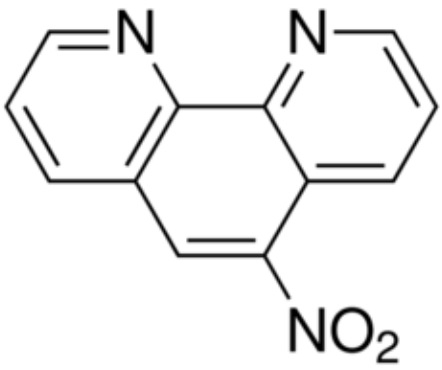

Figure 1.6. 5-Nitro-1, 10-phenanthroline

In this research we are using organic ligands, such as phenanthroline and terpyridine ligands, which are electron donors and are used as strong chelating agents. These ligands have multiple donor sites, which can coordinate to lanthanide ions. The overall goals of this research are to successful coordinate terbium or europium to the nitrogen donor site to sensitive and enhance the luminescence intensity of the lanthanide ions. Enhancing the luminescence of the lanthanide is accomplished by excited state energy transfer from the allowed ligand based excitation to the lanthanide f-excited level. A current interest in our lab is rationally designing system where the weak lanthanide emission can be enhanced through a cooperative effect of multiple donor systems. Hence, in this project we are aspiring to coordinate a transition metal complex as the second donor. The potassium dicyanoaurate (I) is thus coordinated as a second donor to the lanthanide ion. In doing this we are hoping to see energy transfer from the dicyanoaurate (I) to the lanthanide excited state which may assist in the enhancement of the luminescence efficiency of the lanthanide ion.

CHAPTER 2

Experimental Methods

2.1 Materials

Solvents used in this study for synthesis are acetonitrile, ethanol, methanol, and distilled water. Metals used $EuCl_3 \bullet 6H_2O$, and $TbCl_3 \bullet 6H_2O$ hexahydrate. Selected ligands used were 5-Nitro-1, 10-phenanthroline, 4'-(4-methylphenyl)-2, 2':6', 2''-terpyridine (Terpy), 2, 2′-Dithiobis (5-nitropyridine) (DTNP), and potassium dicyanoaurate (I) ($KAu(CN)_2$). All chemicals were from Sigma-Aldrich and used without further purification. 1, 3, 5-triaza-7-phosphaadamantane-7-oxide (TPAO) was prepared as described in the literature [20].

2.2 Experimental

2.2.1 Synthesis of $[Tb(H_2O)_4(Au(CN)_2)(C_{22}H_{17}N_3)(TPAO)]Cl_3$,1 This synthesis was carried out using 0.0710g of TPAO, 0.0720g of terpy, 0.0500g of $TbCl_3 \bullet 6H_2O$, and 0.0819g of $KAu(CN)_2$. terpy and TPAO were placed in a 50mL round bottom flask and dissolved in 5mL of MeCN and 5mL MeOH allowed to heat and stir for 5 min $TbCl_3$ and $KAu(CN)_2$ were placed in a separate vial and 4 mL of EtOH and 2 mL of distilled water was added and heated for 5 minutes. Then $TbCl_3$ and $KAu(CN)_2$ were placed into a beaker. Then slowly added the TPAO and Terpy solution, then covered with parafilm and let slowly evaporate.

2.2.2 Synthesis of $[Eu(H_2O)_4(Au(CN)_2)(C_{22}H_{17}N_3)]Cl_3$, 2. A 0.1164g of terpy, 0.1179g of $EuCl_3$, and 0.1061g of $KAu(CN)_2$ was measured out and placed in a 25mL round bottom flask. Then add 5mL of EtOH, 5mL of MeOH, and 5mL of acetone. Allowed solution to heat and stirred for 5 minute. The solution was then filtered and covered with parafilm and allowed to slowly evaporate.

2.2.3 Synthesis of $[Tb(H_2O)_4(Au(CN)_2)(C_{22}H_{17}N_3)]Cl_3$,3. A 0.1202 g of terpy, 0.0817g of $TbCl_3$, and 0.0800g of $KAu(CN)_2$ was measured out and placed in a 25 mL round bottom flask. Then add 5mL of EtOH, 5mL of MeOH, and 5 mL of acetone. Allowed solution to heat and stir for 5 minute. The solution was then filtered and covered with parafilm and allowed to slowly evaporate.

2.2.4 Synthesis of $[Eu(H_2O)_4Au(CN)_2(Phen)]Cl_3$,4. A 0.01237g of Phen, 0.01279g of $EuCl_3$, and 0.01191g of $KAu(CN)_2$ was measured out and placed in a 25mL round bottom flask. Then add 5mL of EtOH, 5mL of MeOH, and 5mL of acetone. Allowed solution to heat and stir for 5 minute. The solution was then filtered and covered with parafilm and allowed to slowly evaporate.

2.3 Spectroscopic Methods

The characterization of the research samples where done using various techniques, amongst the spectroscopic methods, which includes IR, Raman, and luminescence instruments. The IR spectra were collected using Shimadzu IRPrestige21 Fourier-Transform infrared spectrophotometer using potassium bromide (KBr) pellets. Steady-state emission and excitation were collected on a Photon Technology (PTI) photomultipler detection system. Raman data was collected using Horiba XploRA Raman Confocal Microscope System.

2.4 X-ray Crystallographic Studies

The X-ray data was collected using the SMART X2S single X- ray diffractometer using the Mo-Kα radiation. X-ray quality crystals were selected from under a microscope to check the polarizability and color. The single crystals are measured in mm under the microscope. The single crystal is mounted on a pin and loaded into the instrument. The SMART X2S automatically places the crystal on the goniometer head, aligns the sample and begins collecting

data on a CD-R. Once data is collected from the CCD detector were interpreted and integrated with the program AXS from Bruker. The structure was solved and refined using the SHELXTL Software Package. The final anisotropic full-matrix least-squares refinement on F2 with variables converged at R1, for the observed data and wR2 for all data. The goodness-of-fit, largest peak in the final difference electron density synthesis and the largest hole with an RMS deviation was considered. On the basis of the final model, the density and F(000) is calculated. Although several crystals were mounted and analyzed in this work, unfortunately none of the targeted compounds crystallized with suitable quality and feature for full data collection and/or provided acceptable solutions.

2.5 Photoluminescence Measurement

The luminescence spectra were collected using a Photon Technology International (PTI) spectrometer (model QM-7/SE). The system uses a high intensity Xe source for excitation. Selection of excitation and emission wavelengths are conducted by means of computer controlled, autocalibrated “QuadraScopic” monochromators and are equipped with aberration corrected emission and excitation optics. Signal detection is accomplished with a PMT detector (model 928 tube) that can work either in analog or digital (photon counting) modes. All of the emission spectra presented are corrected to compensate for wavelength dependent variation in the system on the emission channel. The emission correction files which were generated by comparison of the emission channel response to the spectrum of a NIST traceable tungsten light were used as received from Photon Technology International (PTI). The emission correction was conducted in real time using the PTI provided protocol. The instrument operation, data collection, and handling were all controlled using the advanced FeliX32 fluorescence spectroscopic package. The steady state emission and excitation spectra were collected upon

continuous excitation (without introducing any time delay). The PTI system uses a high intensity xenon lamp for excitation sources. Signal detection is accomplished with a PMT detector. This PMT detector can work either in analog or digital modes. However, digital (photon counting) modes are used in this research. Data manipulation was achieved by the FeliX32 fluorescence package. This instrumentation was set up in a dark room to avoid possible interference from visible light. Samples were introduced into the luminescence instrument by means of sealed borosilicate capillary tubes.

2.6 Raman Studies

Raman data were collected using the Horiba XploRA Raman Confocal Microscope System. Raman spectroscopy techniques are used to observe vibrational, rotational, and other low-frequency modes in a system. One thing that Raman systems rely on is inelastic scattering of the monochromatic light. The monochromatic light usually comes from the laser in the near infrared, near UV or visible range. The laser light interacts with phonons and molecular vibrations resulting in the energy of the laser photons being shifted. The shift that occurs gives information about the vibrational modes.

CHAPTER 3

Results

3.1 Infrared, photoluminescence, and Raman studies of compound 1

3.1.1 Infrared spectroscopy of 1. Figure 3.1 shows a weak band at 2146 and 2156 cm^{-1} assignable to the CN stretching from $Au(CN)_2^-$. The weak band at 2983 cm^{-1} and 3001 cm^{-1} is due to the ν_{CH} symmetric stretch for a sp^3 hybridized bond. The broad band around 3320cm^{-1} is due to ν_{OH}, which could be due to the solvents of choice and/or coordinated H_2O.

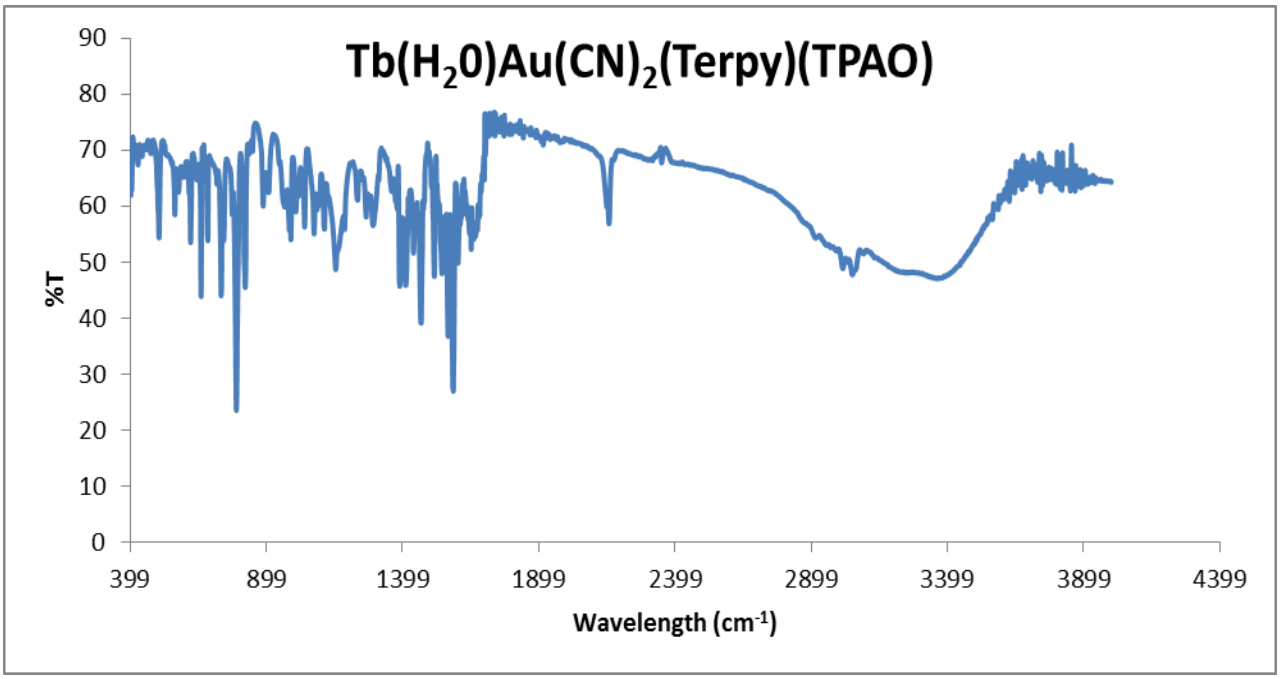

Figure 3.1. Infrared spectrum of compound **1**

3.1.2 Raman studies of 1. The Raman spectrum of compound 1 shown below and observed at 2165 cm^{-1}confirms the coordination of the cyanide group to the lanthanide center as can be seen in Figure 3.2. The stretching frequency was observed at a blue shifted position when compared with the uncoordinated CN stretch in $KAu(CN)_2$ which is usually observed at ~ 2145 cm^{-1}.

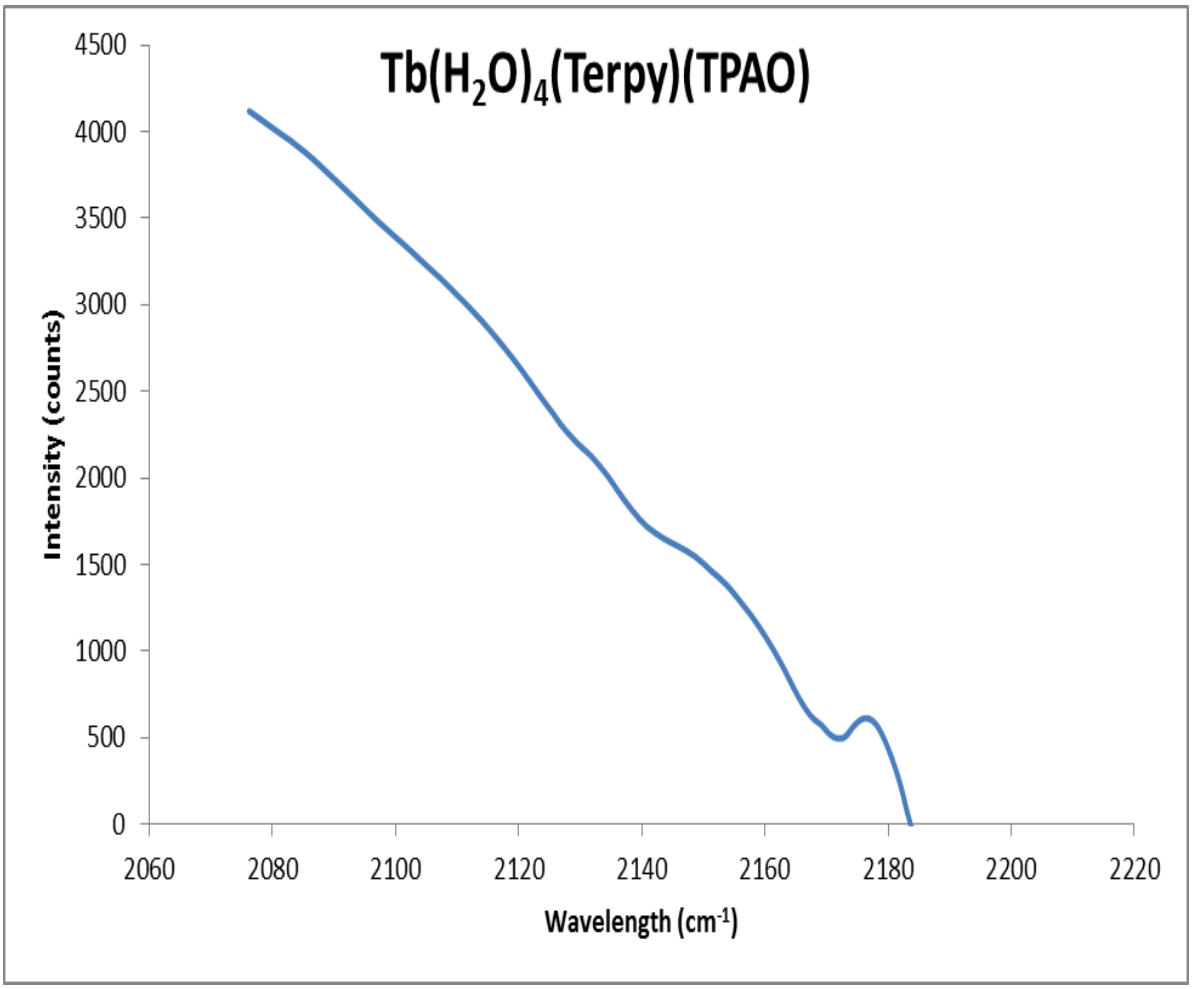

Figure 3.2. Raman spectrum of **1**

3.1.3 Photoluminescence studies of compound 1. The luminescence data of **1** shows the f-f characteristic transitions of Tb^{3+} in the spectra obtained. The emission spectrum of **1** was collected at room temperature in a range of 450 nm to 625 nm upon excitation at 378 nm, which is shown in Figure 3.3 below. The most intense band is at 540 nm (hypersensitive band) when excited at 378 nm, which corresponds to $^5D_4 \rightarrow {}^7F_5$ transition of Tb^{3+}. Figure 3.3 also show other well defined brands at 483, 578, and 615 nm, which are also characteristic of Tb^{3+}. When collecting the spectrum under liquid nitrogen the Tb^{3+} profile intensity increases, shown in Figure 3.4 below.

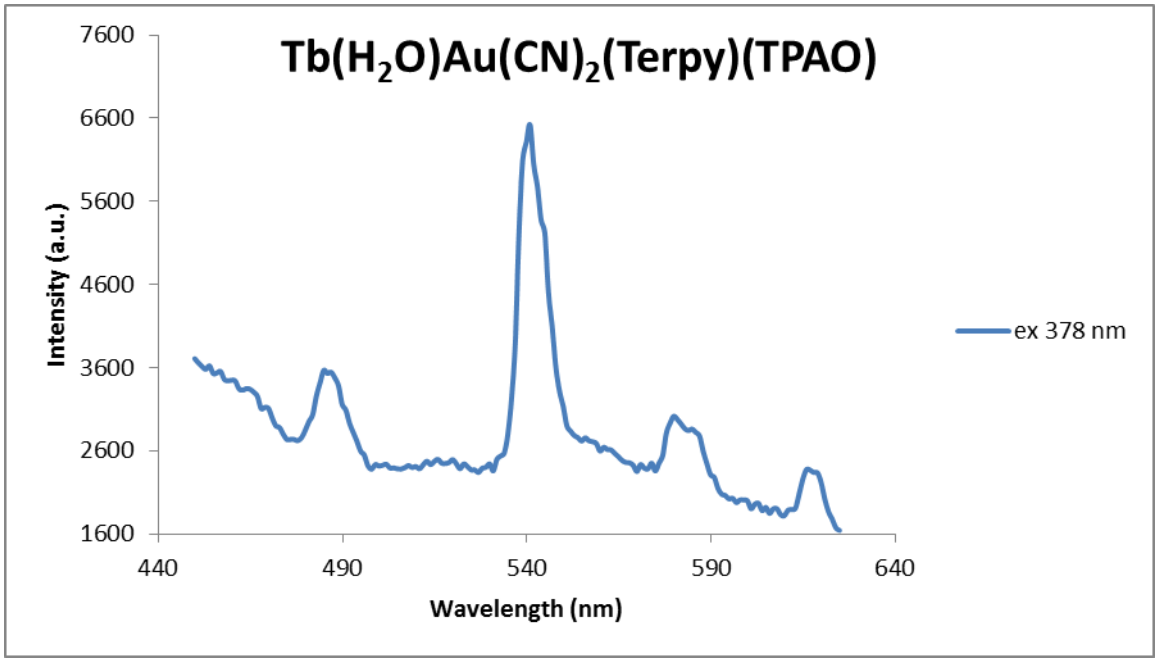

Figure 3.3. Emission spectrum of **1**collected at room temperature upon excitation 378nm

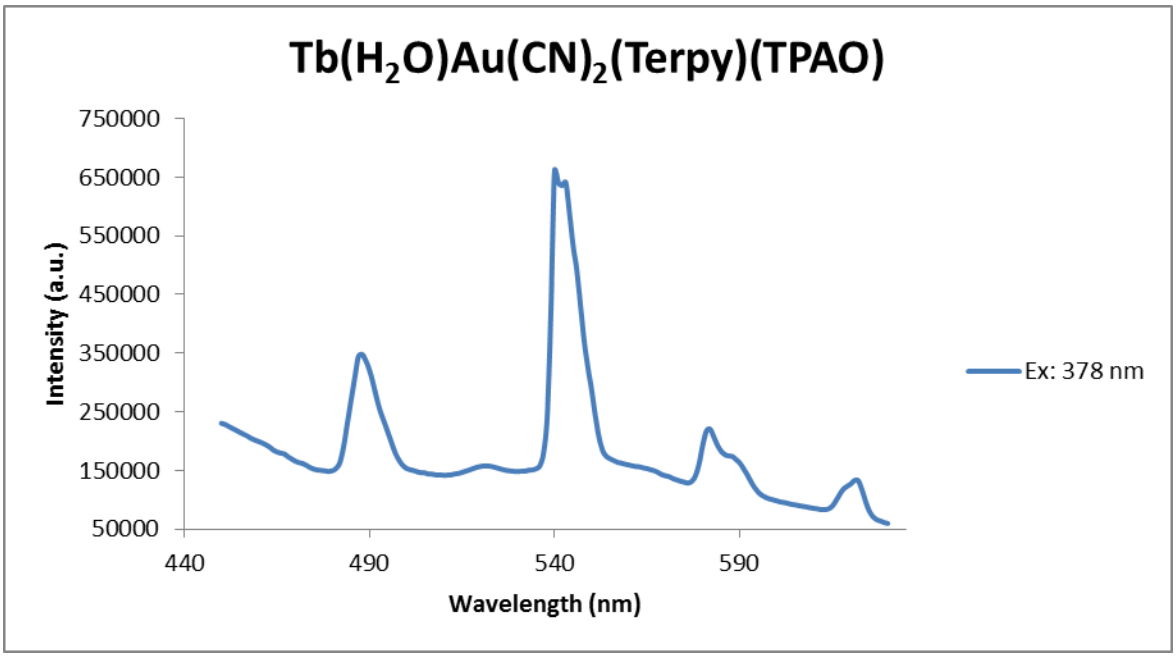

Figure 3.4. Emission spectrum of **1** collected under Liq. N_2 and excited at 378 nm

The emission spectrum of **1** was collected at room temperature in a range of 440 nm to 625 nm upon excitation at 343, 350, and 385 nm, which are shown in Figures 3.4, 3.6, and 3.7 below. Figure 3.4 and 3.6 was collected at room temperature. Both spectra show the

hypersensitive band is at 542 nm when excited at 343 nm and 350 nm, which corresponds to $^5D_4 \rightarrow ^7F_5$. When exciting the two spectra under liquid nitrogen there is no difference except an increase in intense, shown in Figures 3.5 and 3.7. Figure 3.8 show s hypersensitive and at 541nm when excited at 385 nm. The hypersensitive band for Tb^{3+} corresponds to $^5D_4 \rightarrow ^7F_5$ transition. The peak assignments are listed in Table 3.1, which highlight the corresponding energy and assignment transitions respectively to the wavelengths that are seen in the spectra.

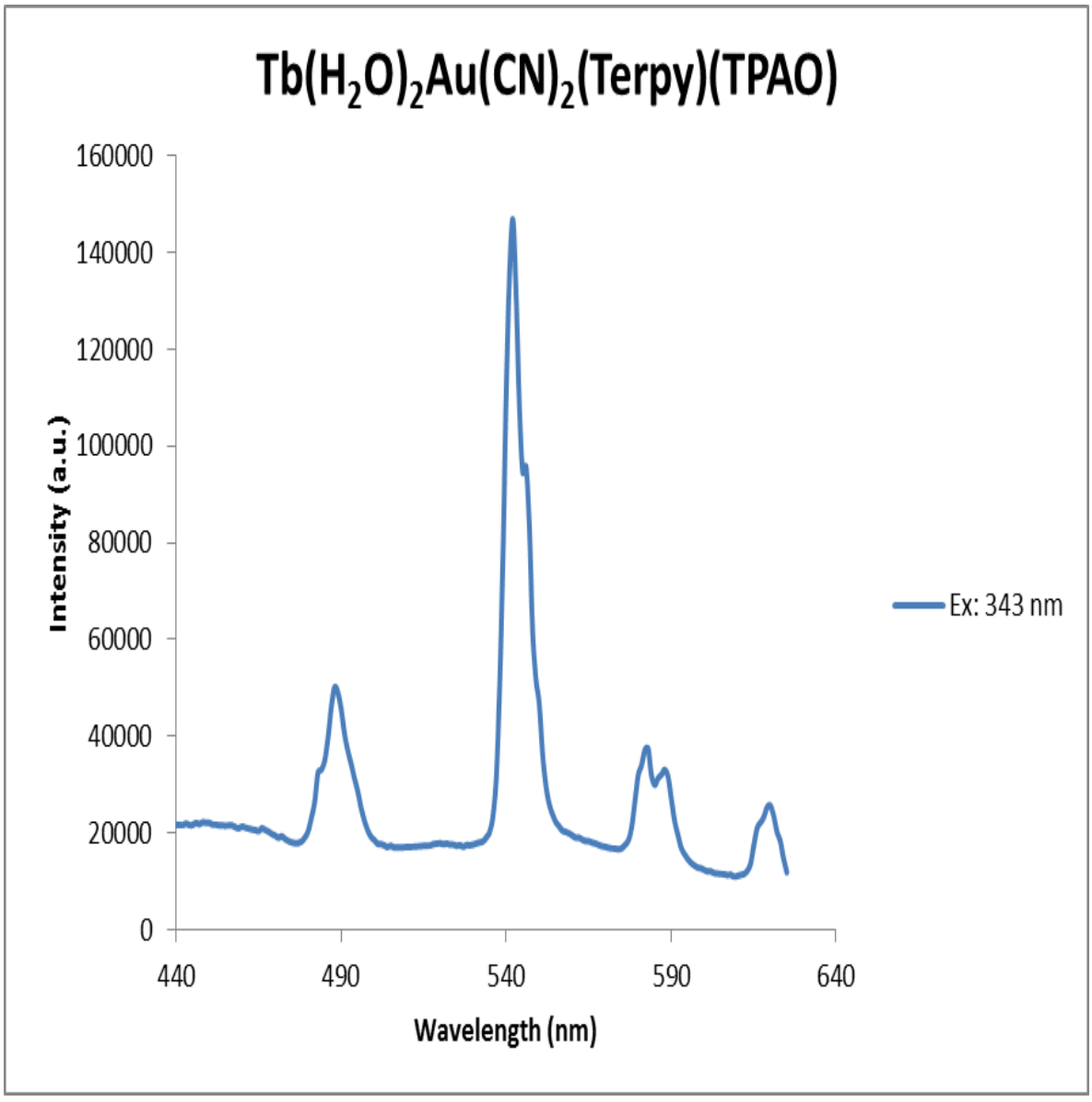

Figure 3.5. Emission spectrum of **1** collected at room temperature upon excitation at 343 nm

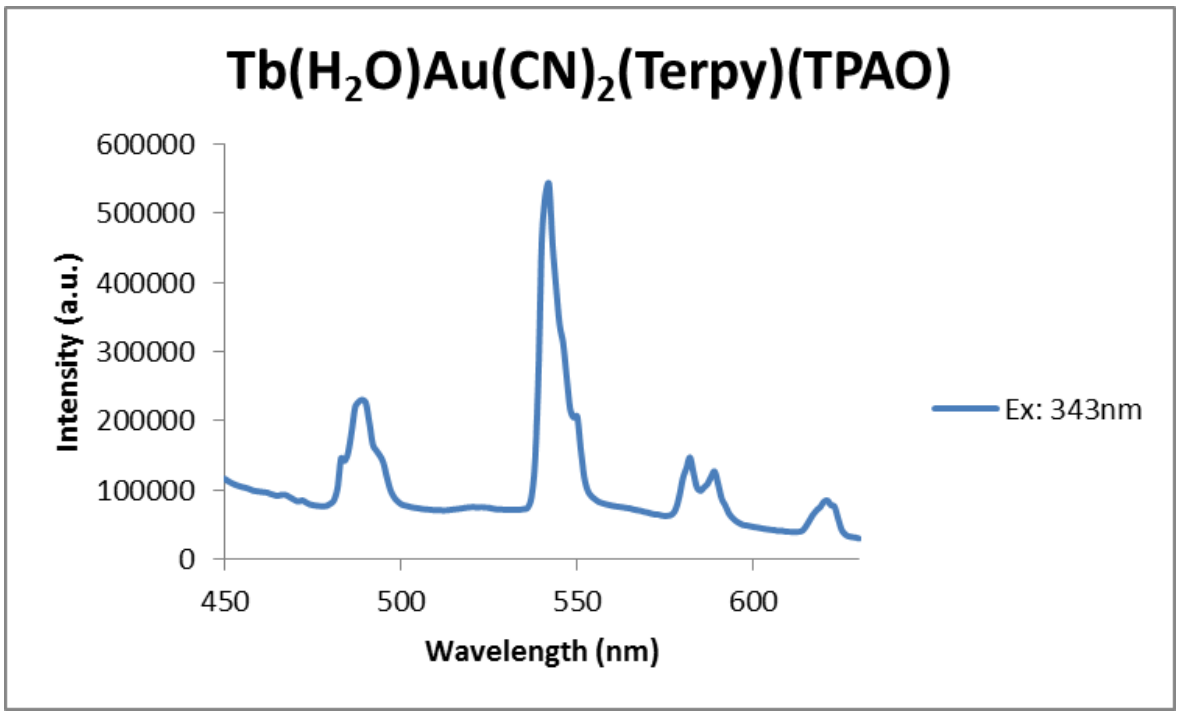

Figure 3.6. Emission spectrum of **1** collected under Liq. N_2 and excited at 343 nm

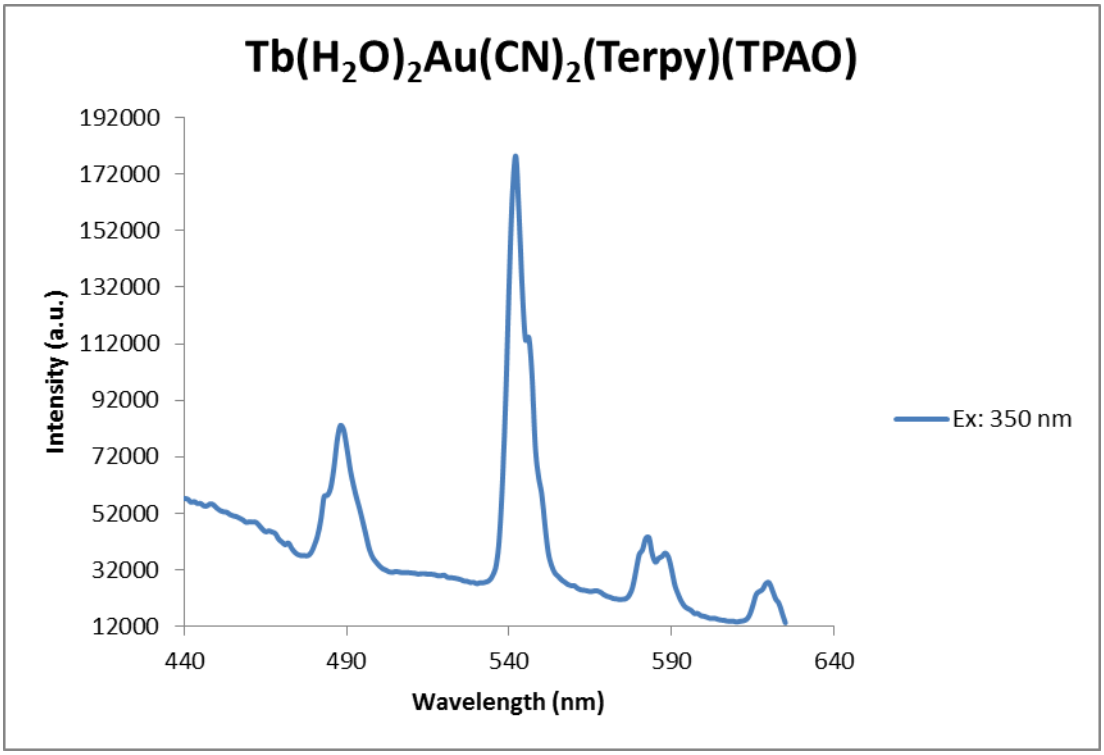

Figure 3.7. Emission spectrum of **1** collected at room temperature and excited at 350 nm

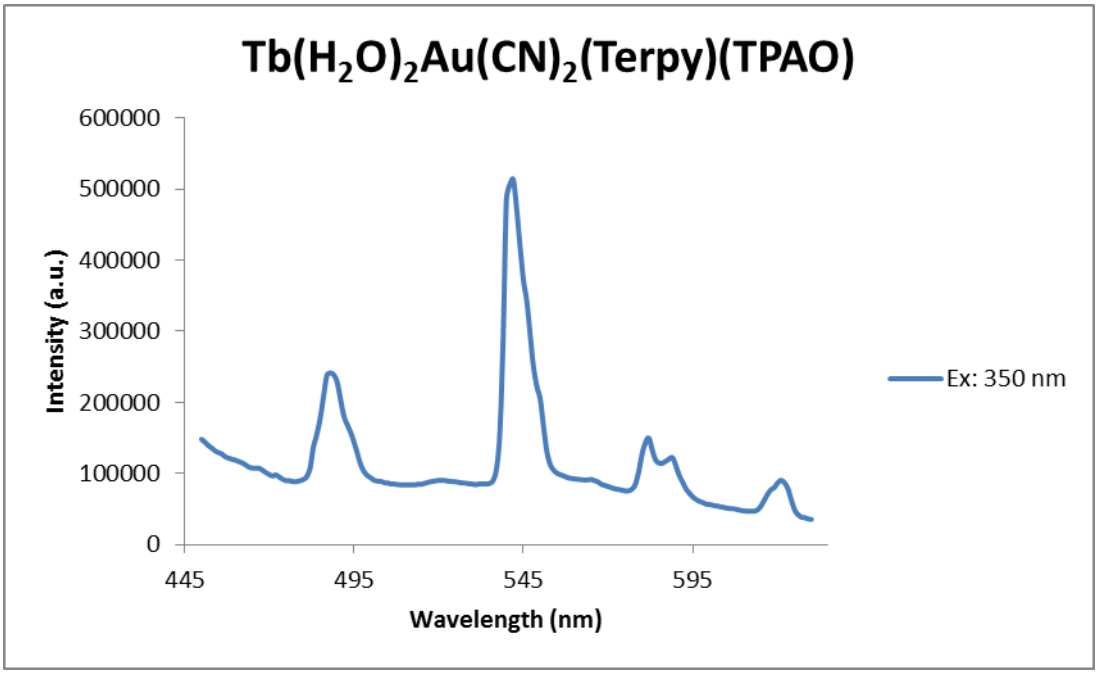

Figure 3.8. Emission spectrum of **1** collected under Liq. N_2 and excited at 350 nm

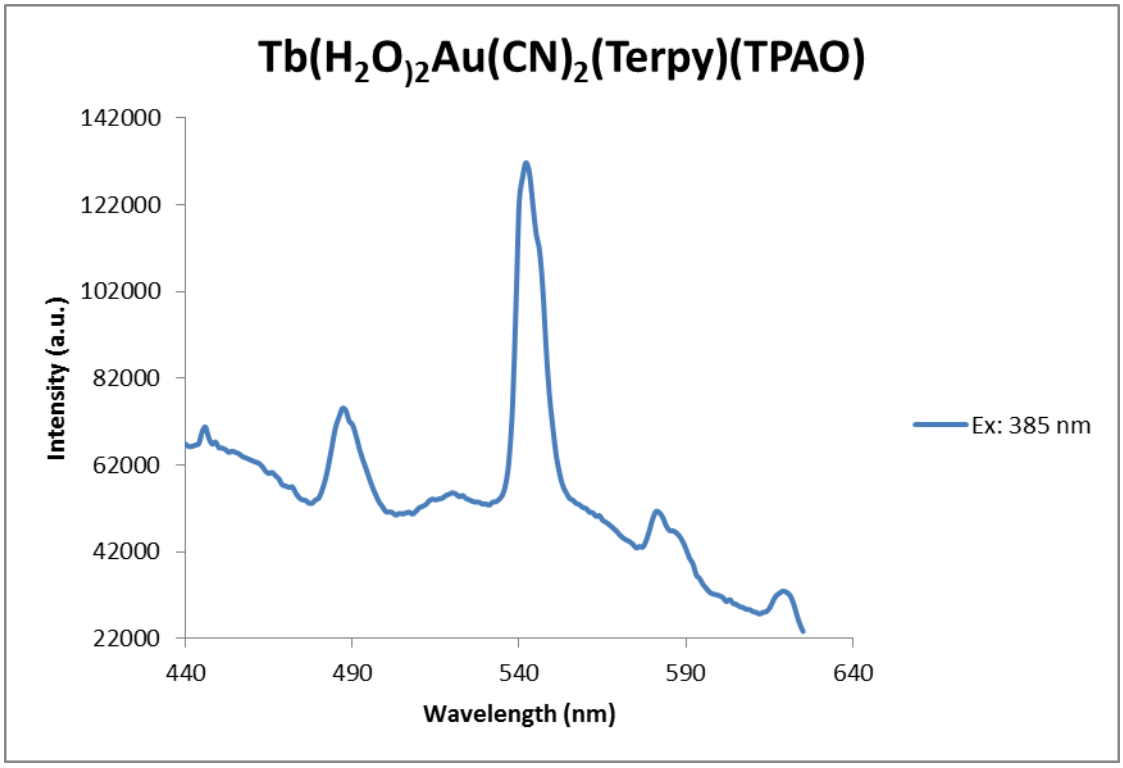

Figure 3.9. Emission spectrum of **1** collected at room temperature upon excitation at 385 nm

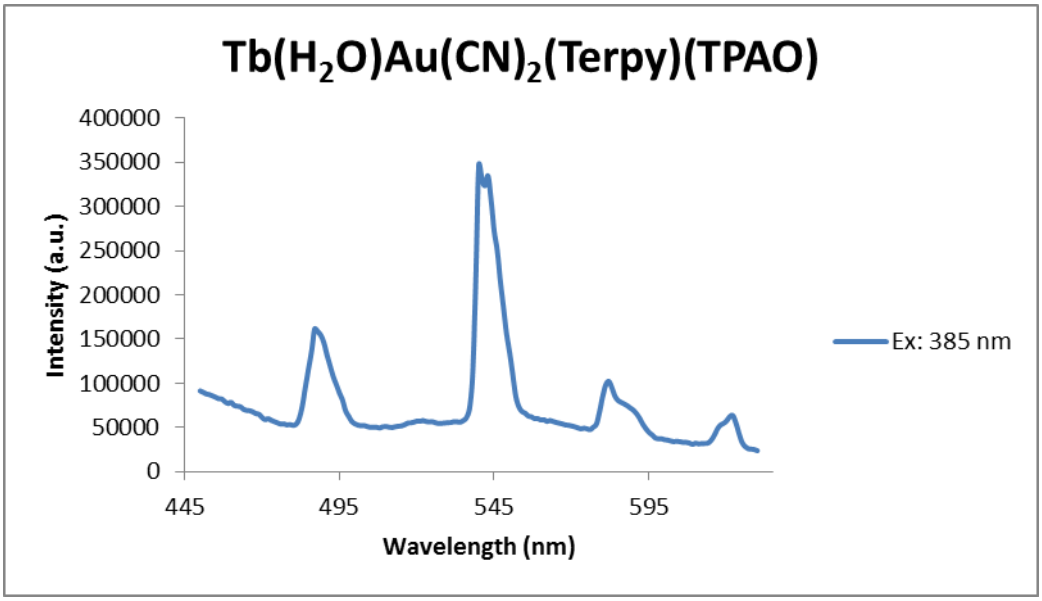

Figure 3.10. Emission spectrum of **1** collected under Liq. N_2 and excited at 385 nm

Table 3.1

*Emission peak positions and assignments for compound **1***

Wavelength (nm)	Wavelength (cm^{-1})	Peak Assignments
485 nm	20619	$^5D_4 \rightarrow {}^7F_6$
541 nm	18484	$^5D_4 \rightarrow {}^7F_5$
579 nm	17271	$^5D_4 \rightarrow {}^7F_4$
582 nm	17182	$^5D_4 \rightarrow {}^7F_3$
615 nm	16260	$^5D_4 \rightarrow {}^7F_2$

The excitation spectrum shown in Figure 3.11 corresponds to compound **1**. The spectrum was collected at room temperature and monitored at 540 nm. The figure shows broad bands centered at 348 nm and 385 nm corresponding to the terpy ligand and $Au(CN)_2^-$, respectively. The weak sharp bands at 404 and 413 nm correspond to f-f transitions within the Tb^{3+}ion. Figure

3.12 was collected under liquid nitrogen shows a broad shoulder around 345 nm and a more intense broad band at 382 nm. The assignments of the peaks are given in Table 3.2, which highlight the transition energies corresponding to the wavelengths that are seen in the spectra.

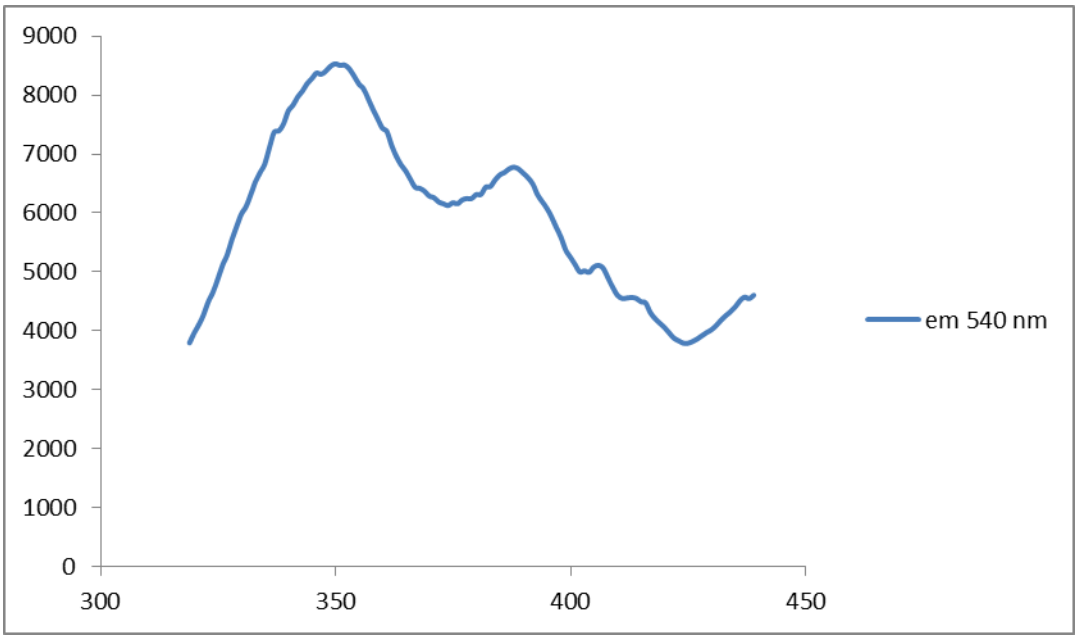

Figure 3.11.Excitation spectrum of **1** collected at room temperature when monitored at 540 nm

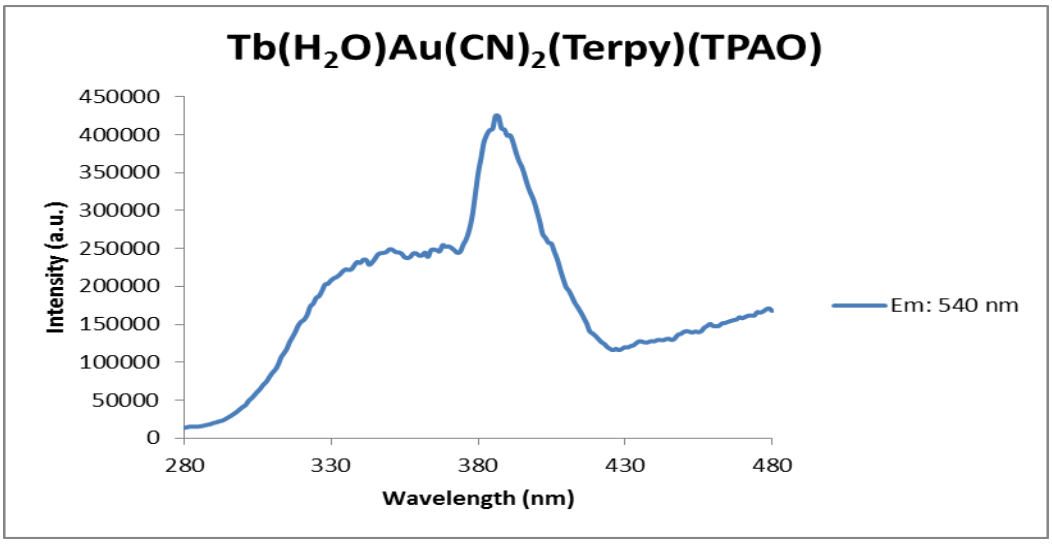

Figure 3.12. Excitation spectrum of **1** collected under Liq. N_2 and monitored at 540 nm

Excitation spectrum of Figure 3.13 was collected at room temperature and monitored at 488 nm. The excitation spectrum shown in Figure 3.13 has two broad bands at 347 and 382 nm

that correspond to the terpy ligand and $Au(CN)_2^-$. Figure 3.14 was collected under liquid nitrogen while monitoring at the 488 nm emission line. The excitation spectrum shows a broad shoulder around 350 and a more intense broad band at 384 nm.

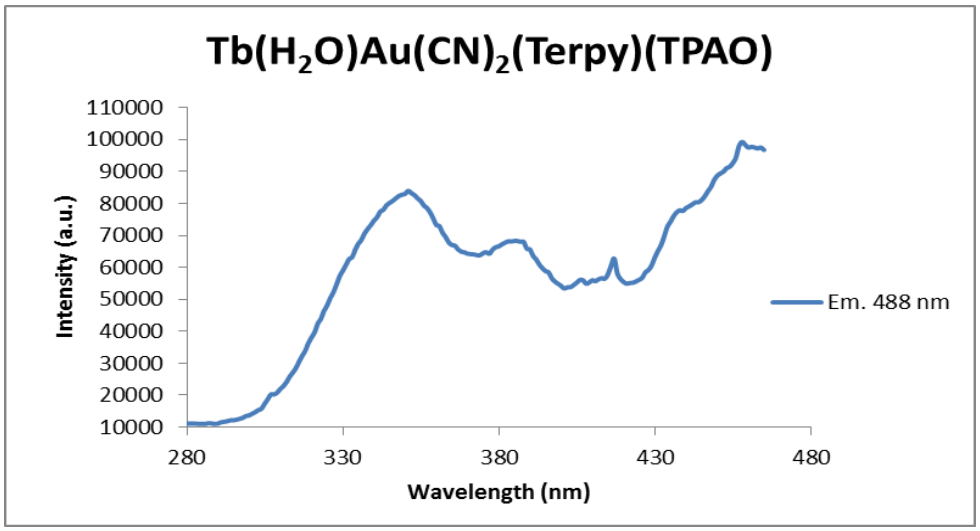

Figure 3.13. Excitation of spectrum of **1** collected at room temperature when monitored at 488nm

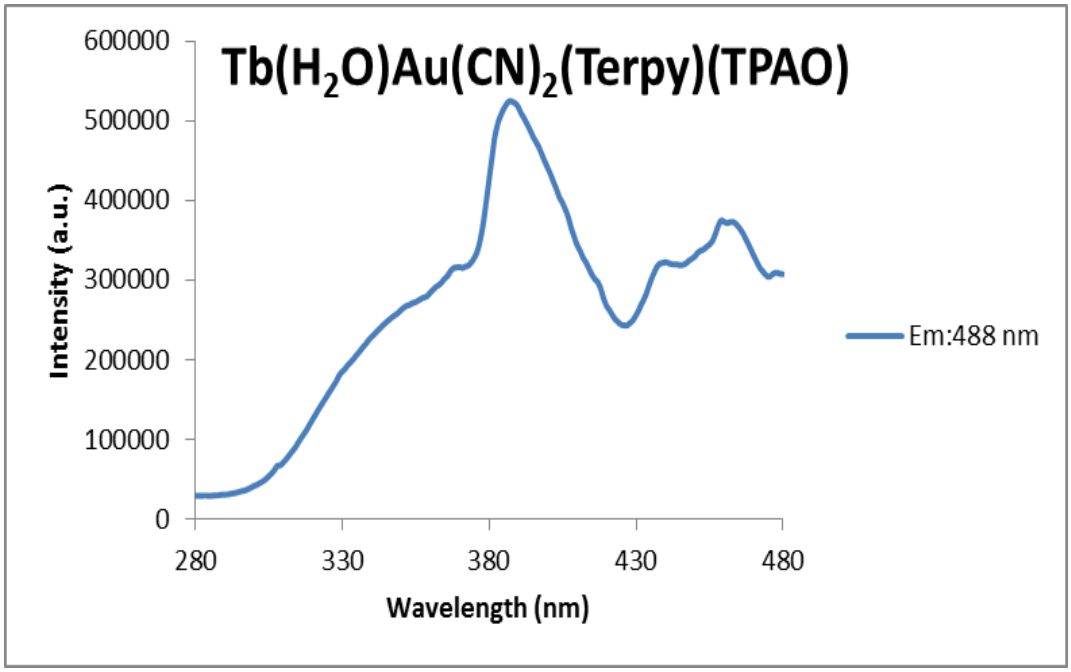

Figure 3.14. Excitation spectrum of **1** collected under Liq. N_2 and monitored at 488 nm

Table 3.1

*Excitation peak positions and assignments for compound **1***

Wavelength (nm)	Wavelength (cm-1)	Peak Assignment
348 nm	28818	$^5D_2 \rightarrow {}^7F_6$
385 nm	25974	$^5D_3 \rightarrow {}^7F_6$
406 nm	24631	$^5D_3 \rightarrow {}^7F_6$
411 nm	24331	$^5D_3 \rightarrow {}^7F_6$

3.2 Infrared, Raman, and photoluminescence's studies of Compound 2

3.2.1 Infrared spectroscopy of 2. Figure 3.15 shows bands at 2158cm^{-1}, 2183cm^{-1}, and 2140cm^{-1} which corresponded to the υ_{CN} stretching. The 2158cm^{-1} band which is a strong band is due to the coordination of the $Au(CN)_2^-$. However, the stretching at 2183cm^{-1} and 2140cm^{-1} are uncoordinated ν_{CN} bonds from $Au(CN)_2^-$. The ν_{OH} stretching around 3320cm^{-1} could be due to the solvent of choice, which are MeOH and EtOH. The ν_{CC} Stretching at around 1604cm^{-1} is due to the methyl group on the aromatic ring.

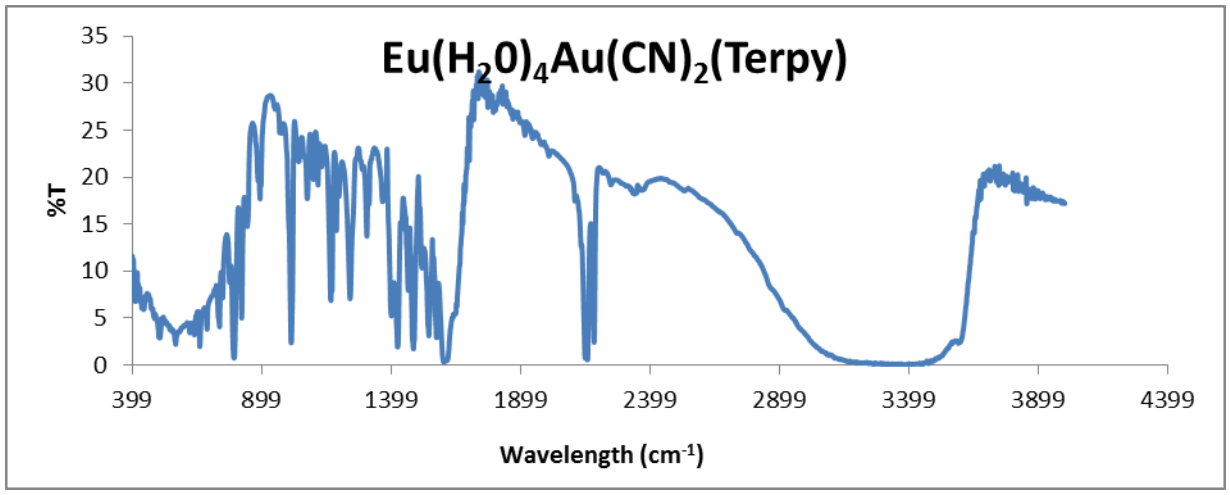

Figure 3.15. Infrared spectroscopy of compound **2**

3.2.2 Raman studies of 2. The Raman spectrum of compound **2** shows the coordination of CN to the Eu^{3+}. The CN stretching peaks are observed at 2138, 2146, and 2179 cm^{-1} as shown in Figure 3.16 below. The former two appear as a doublet.

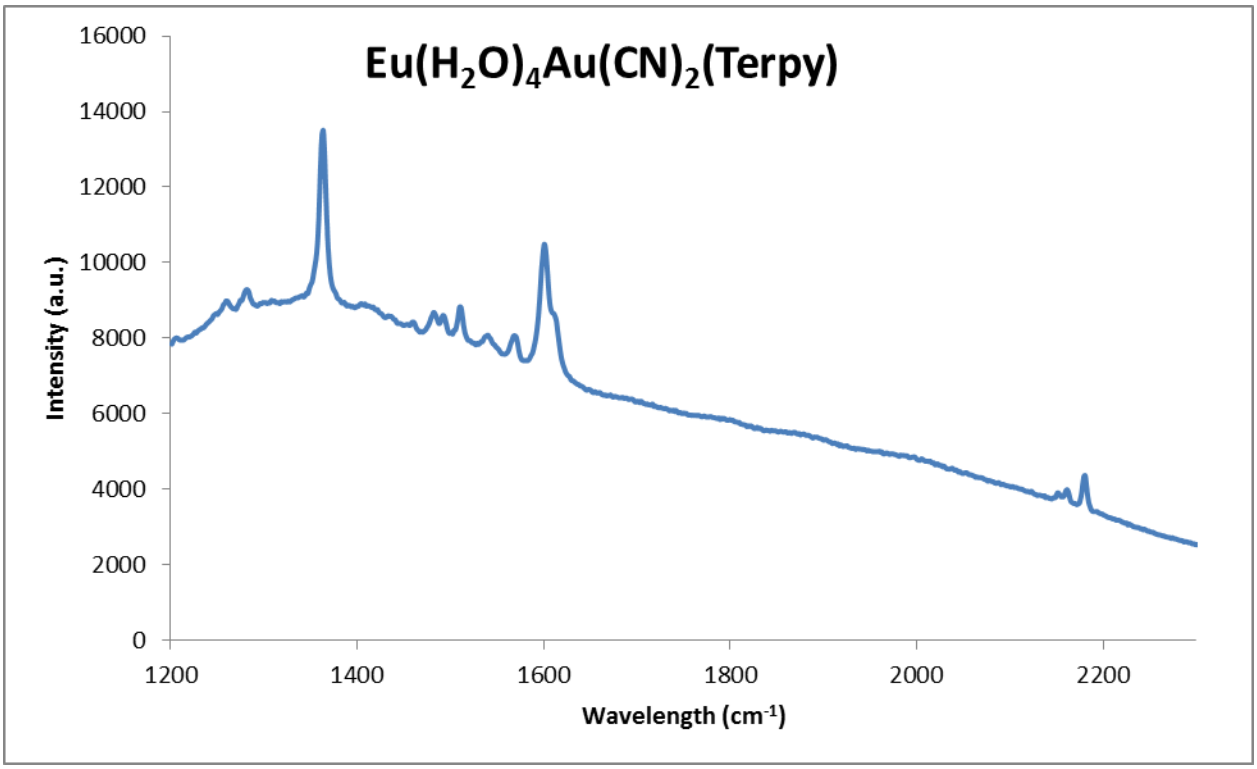

Figure 3.16. Raman Spectrum of **2**

3.2.3 Photoluminescence studies of 2. The emission spectra of **2** were collected at room and liquid nitrogen. The emission spectra of 2 are shown in Figures 3.17 and 3.18. The spectra were collected upon excitation at 378nm and show characteristics of Eu^{3+} bands. The most intense peak is observed at 615 nm corresponding to $^5D_0 \rightarrow {}^7F_2$ transition, which is noted in table 3.3 below. The emission spectra of **2** shown in Figures 3.19 and 3.20 were collected at room temperature and under liquid nitrogen upon excitation at 343nm, showing characteristics of Eu^{3+} bands. The emission spectra of Figure 3.21 and 3.22 were collected at room temperature when exiting it at 385 and 400 nm, which shows the characteristics of Eu^{3+}. Figure 3.22 hypersensitive band is at 611 nm, which corresponds to $^5D_0 \rightarrow {}^7F_3$ transition. Other Eu^{3+} bands are also

observed at 590, 647, 688, and 697 nm. When collecting the emission spectrum under liquid nitrogen the intensity increase which is shown in Figure 3.23 below.

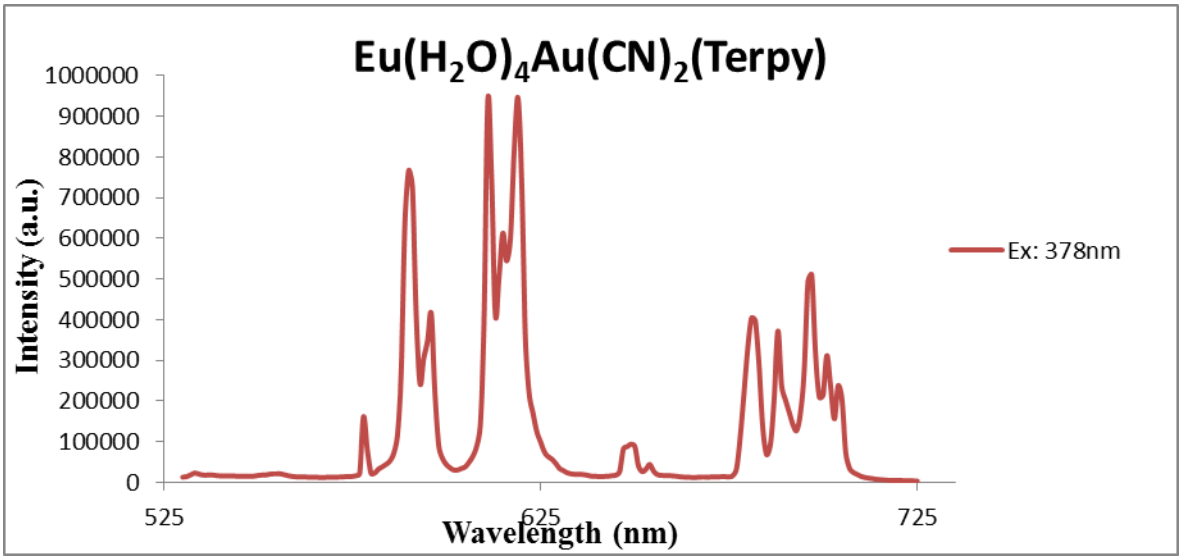

Figure 3.17. Emission spectrum of **2** collected at room temperature upon excitation with 378 nm

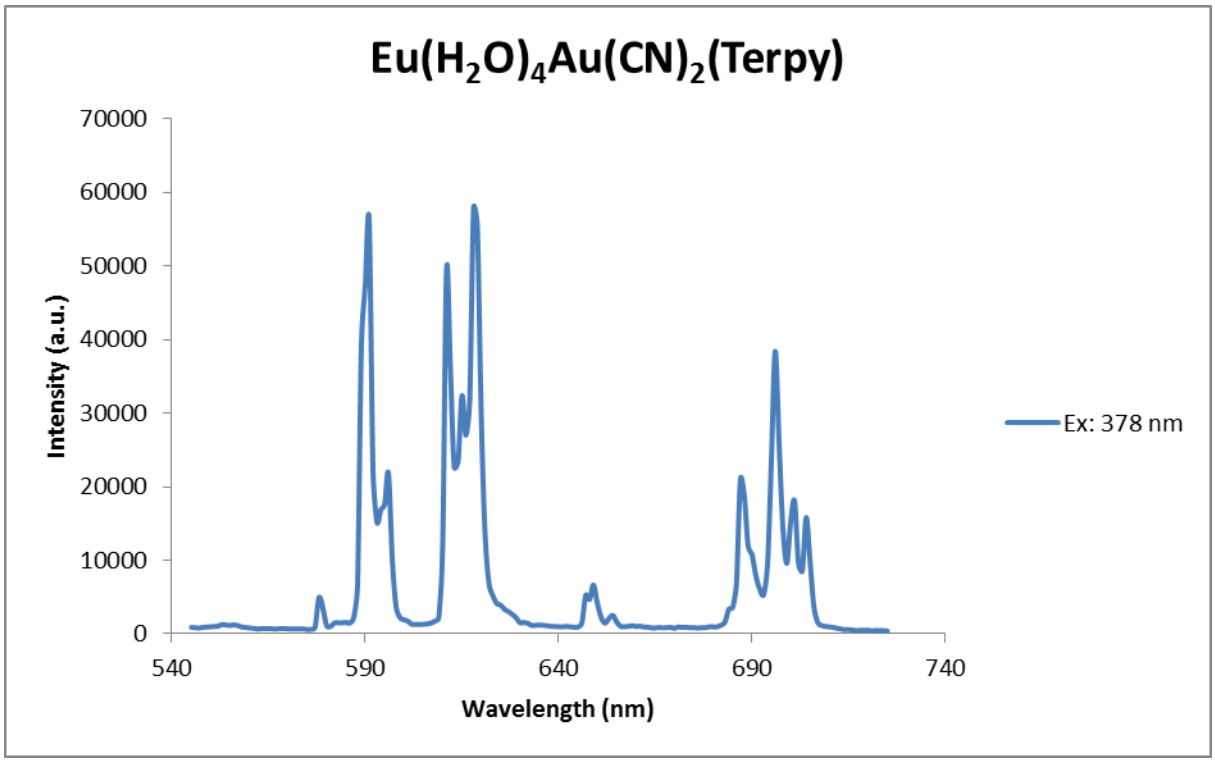

Figure 3.18. Emission spectrum of **2** collected under Liq. N_2 and excited at 378 nm

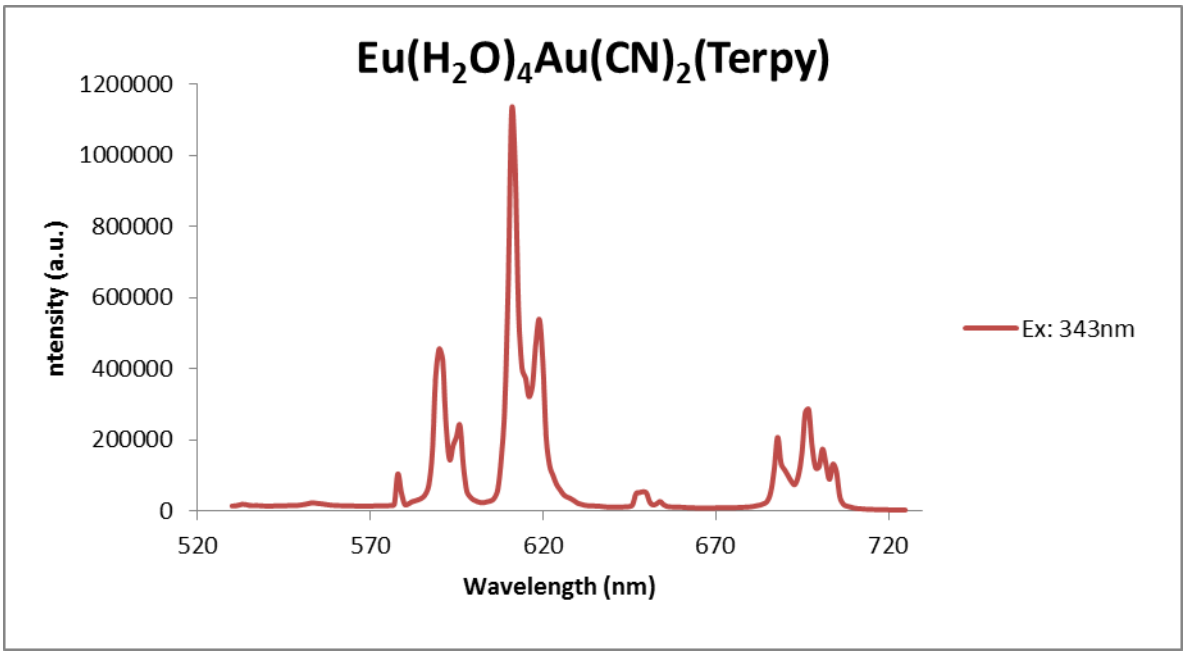

Figure 3.19. Emission spectrum of **2** collected at room temperature upon excitation with 343 nm

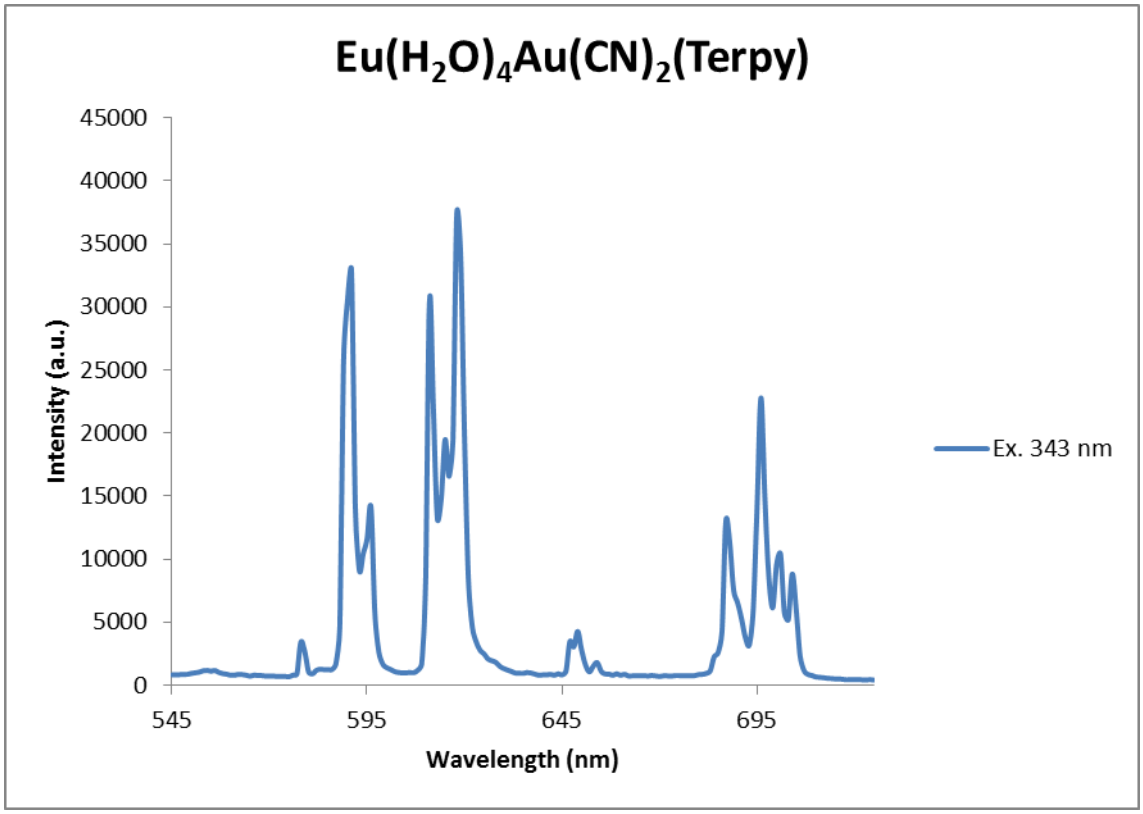

Figure 3.20. Emission spectrum of **2** collected under Liq. N_2 and excited at 343nm

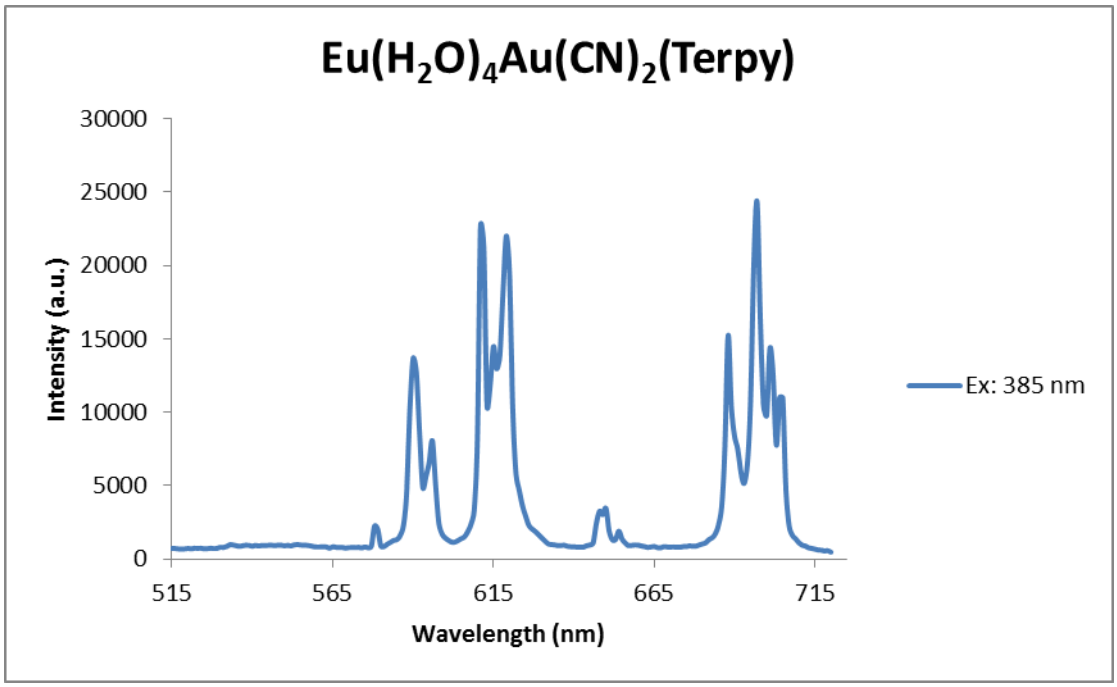

Figure 3.21. Emission spectrum of **2** collected at room temperature upon excitation with 385 nm

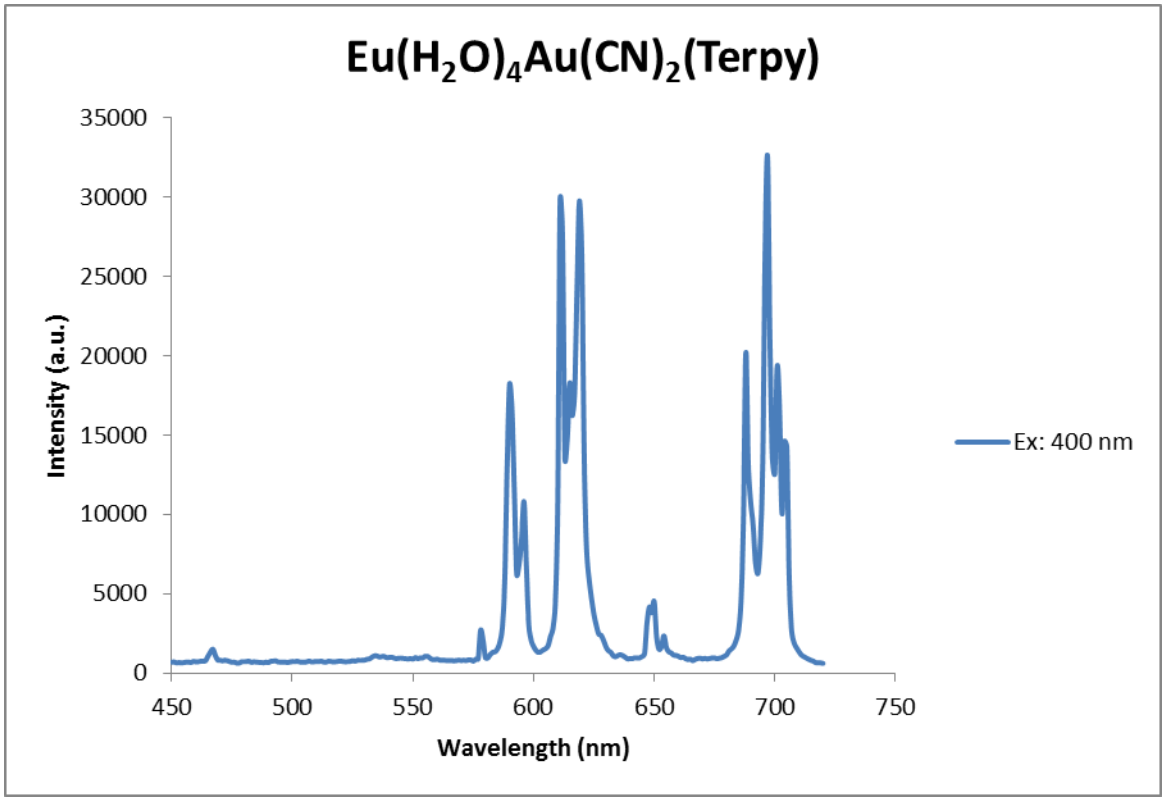

Figure 3.22. Emission spectrum of **2** collected at room temperature upon excitation at 400 nm

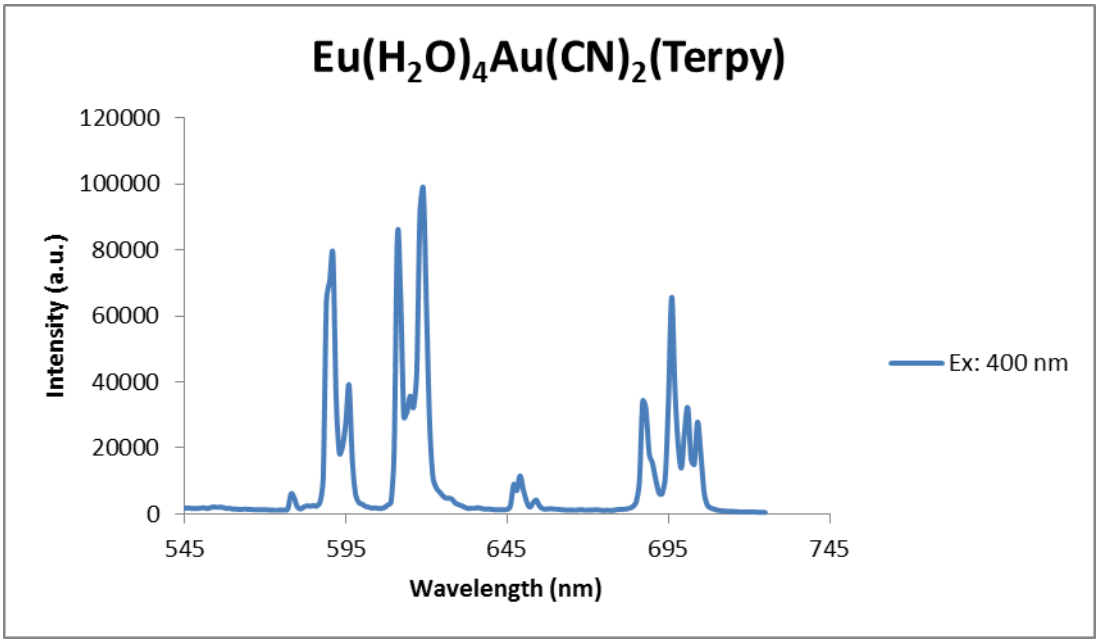

Figure 3.23. Emission spectrum of **2** collected under Liq. N_2 and excited at 400 nm

Table 3.3

*Emission peak positions and assignments for compound **2***

Wavelength (nm)	Wavelength (cm^{-1})	Peak Assignments
578 nm	17301	$^5D_0 \rightarrow {}^7F_0$
590nm	16949	$^5D_0 \rightarrow {}^7F_1$
595nm	16806	$^5D_0 \rightarrow {}^7F_1$
615nm	16260	$^5D_0 \rightarrow {}^7F_2$
620nm	16129	$^5D_0 \rightarrow {}^7F_2$
625nm	16000	$^5D_0 \rightarrow {}^7F_2$
649nm	15408	$^5D_0 \rightarrow {}^7F_3$
653nm	15314	$^5D_0 \rightarrow {}^7F_3$
680nm	14706	$^5D_0 \rightarrow {}^7F_4$

Table 3.3

Cont.

690nm	**14493**	**$^5D_0 \rightarrow {}^7F_4$**
696nm	14367	$^5D_0 \rightarrow {}^7F_5$
702nm	14245	$^5D_0 \rightarrow {}^7F_5$
710nm	14084	$^5D_0 \rightarrow {}^7F_5$

All of the excitation spectra of **2** were collected at room temperature and liquid nitrogen. Figures 3.24, 3.25, and 3.26 were directly excited at one of Eu^{3+} characteristic bands. The excitation spectra for compound **2** show broad bands that are uncharacteristic of f-f transitions. All of the excitation spectra for compound **2** contain sharp f-f transition bands around 430nm.

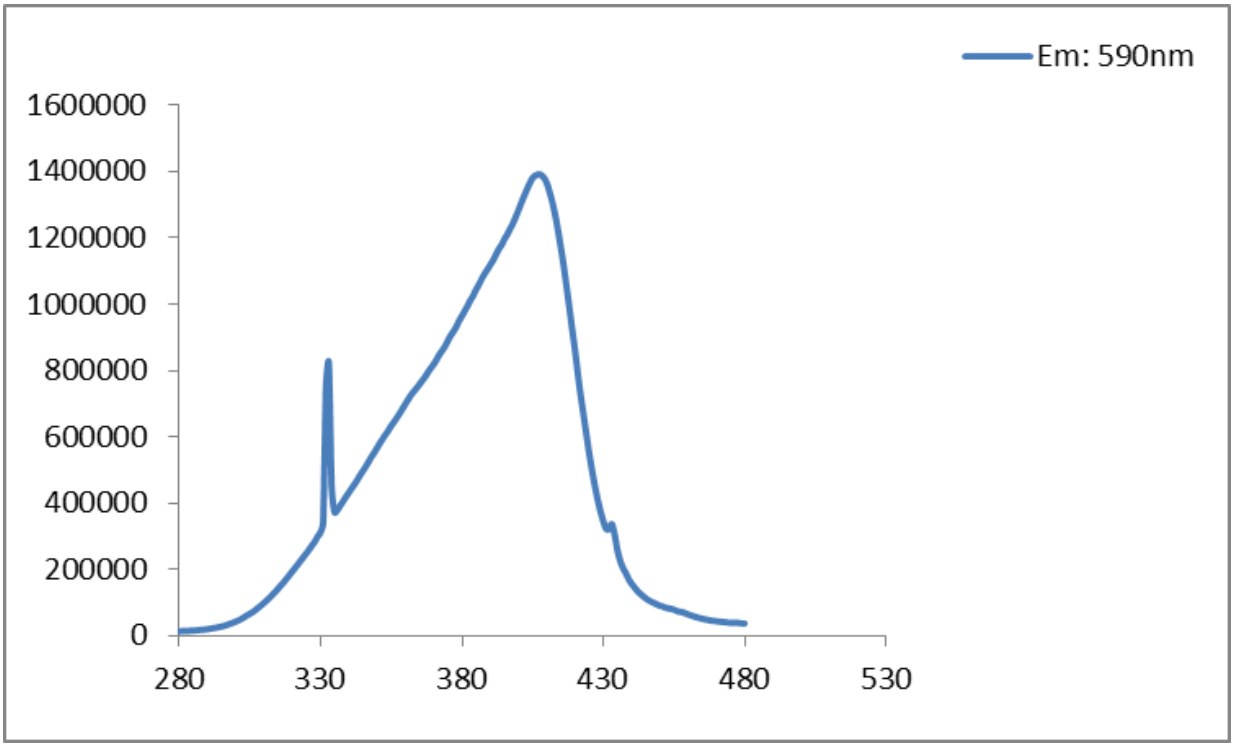

Figure 3.24. Excitation spectrums of **2** when monitored at 590 nm

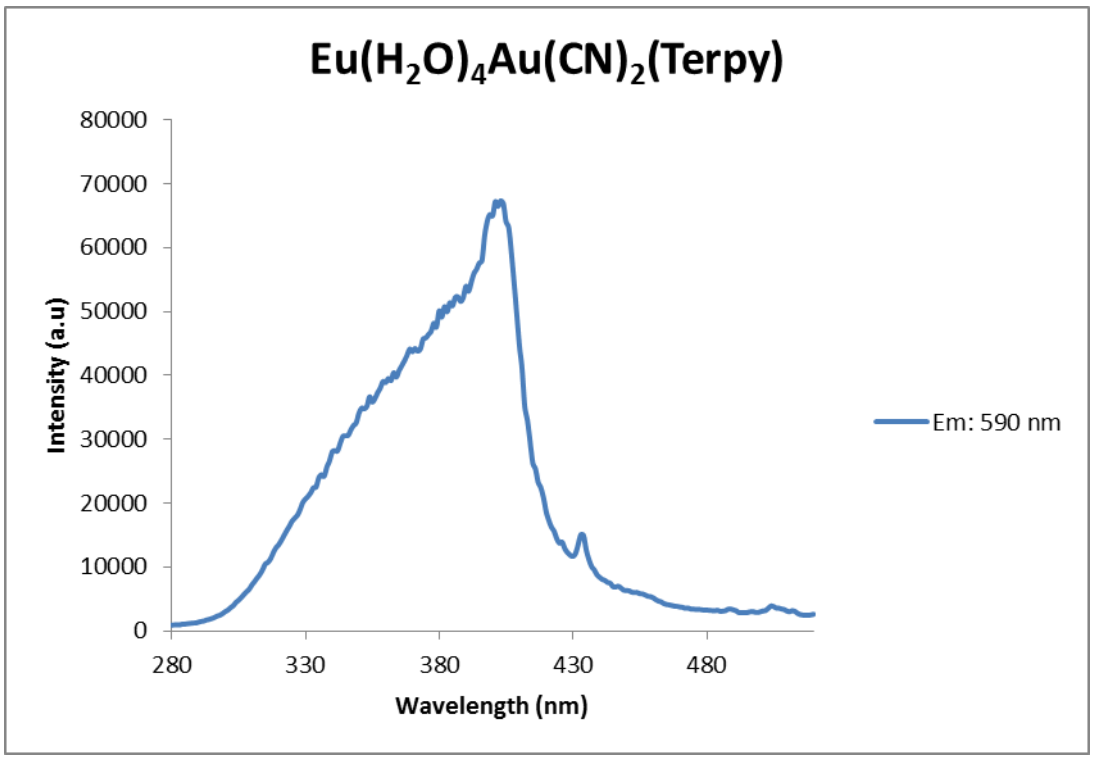

Figure 3.25. Excitation of **2** collected under Liq. N_2 and monitored at 590nm

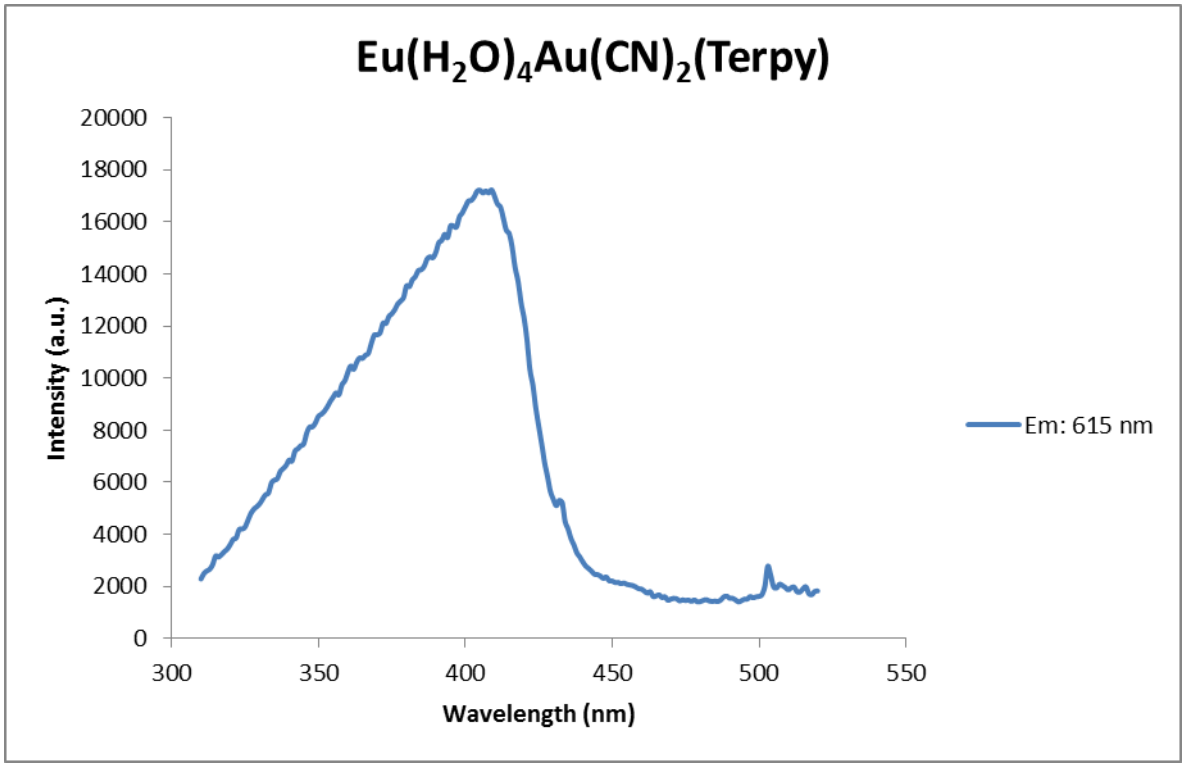

Figure 3.26. Excitation spectrum of **2** when monitored at 615 nm

Table 3.2

*Emission peak positions and assignments for compound **2***

Wavelength (nm)	**Wavelength (cm-1)**	**Peak Assignment**
402 nm	24875	$^5L_6 \rightarrow {}^7F_0$

Another emission spectrum of compound **2** was collected at room temperature, while exciting at 381 nm and ranging from 525 nm to 700 nm to determine if there is any energy transfer from the ligand to the metal ion. When exciting at 381 nm characteristic bands from the Eu^{3+} are observed around 615 nm, as shown in Figure 3.27.

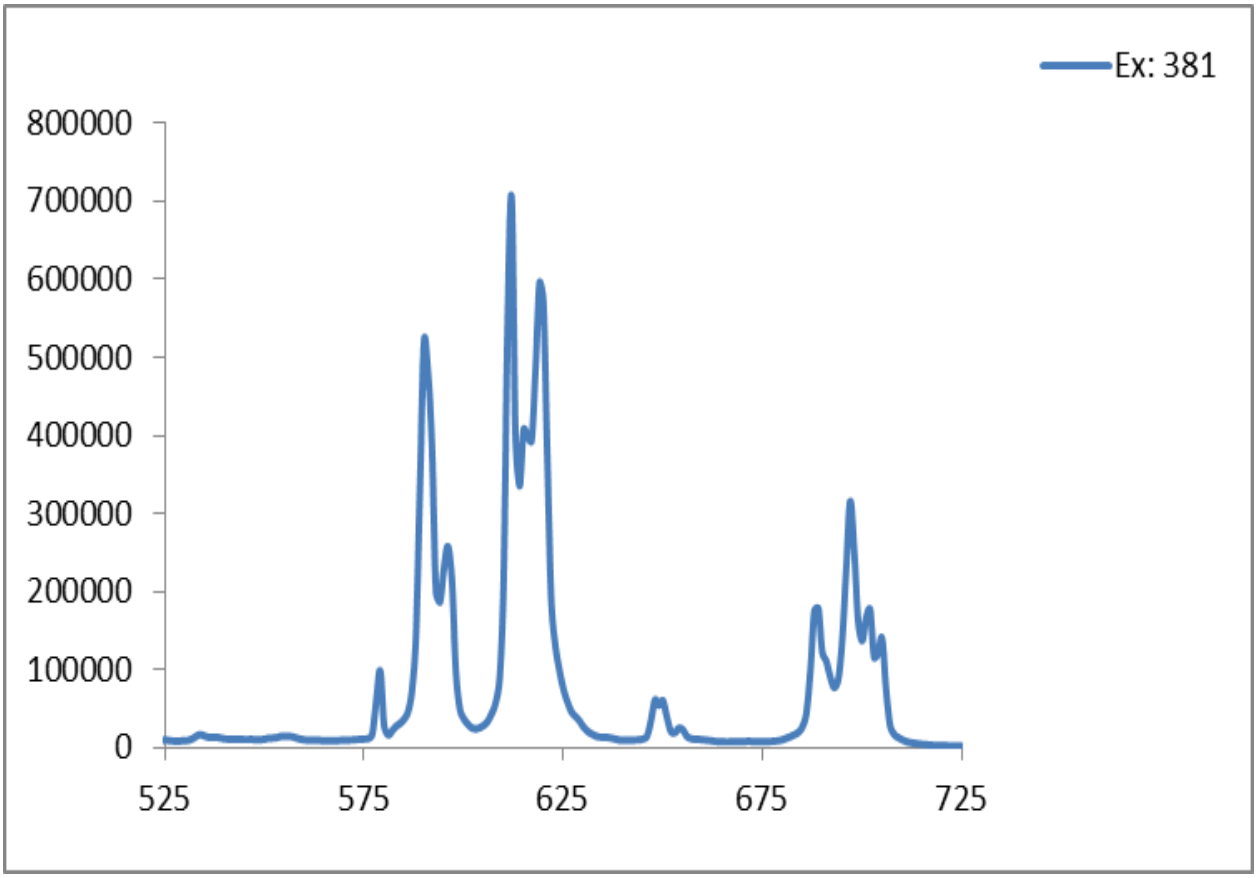

Figure 3.27. Emission spectrum of **2** collected at room temperature upon excitation with 381 nm

3.3 Infrared, photoluminescence, and Raman studies of Compound 3

3.3.1 Infrared spectroscopy of 3. Figure 3.28 shows bands at 2151cm^{-1}, 2217cm^{-1}, and 2226cm^{-1} which corresponded to the ν_{CN} stretching. The medium stretching at 2151cm^{-1} corresponds to the coordinated CN from $Au(CN)_2^-$. There is a strong broad ν_{OH} band at 3308cm^{-1}, which could possibly be due to the solvent of choice, which are MeOH and EtOH and MeCN. There is also overlapping of sp^3 hybridization of ν_{CH} at 3196 cm^{-1}. The strong ν_{CC} stretching at 1625cm^{-1} is due to the aromatic ring.

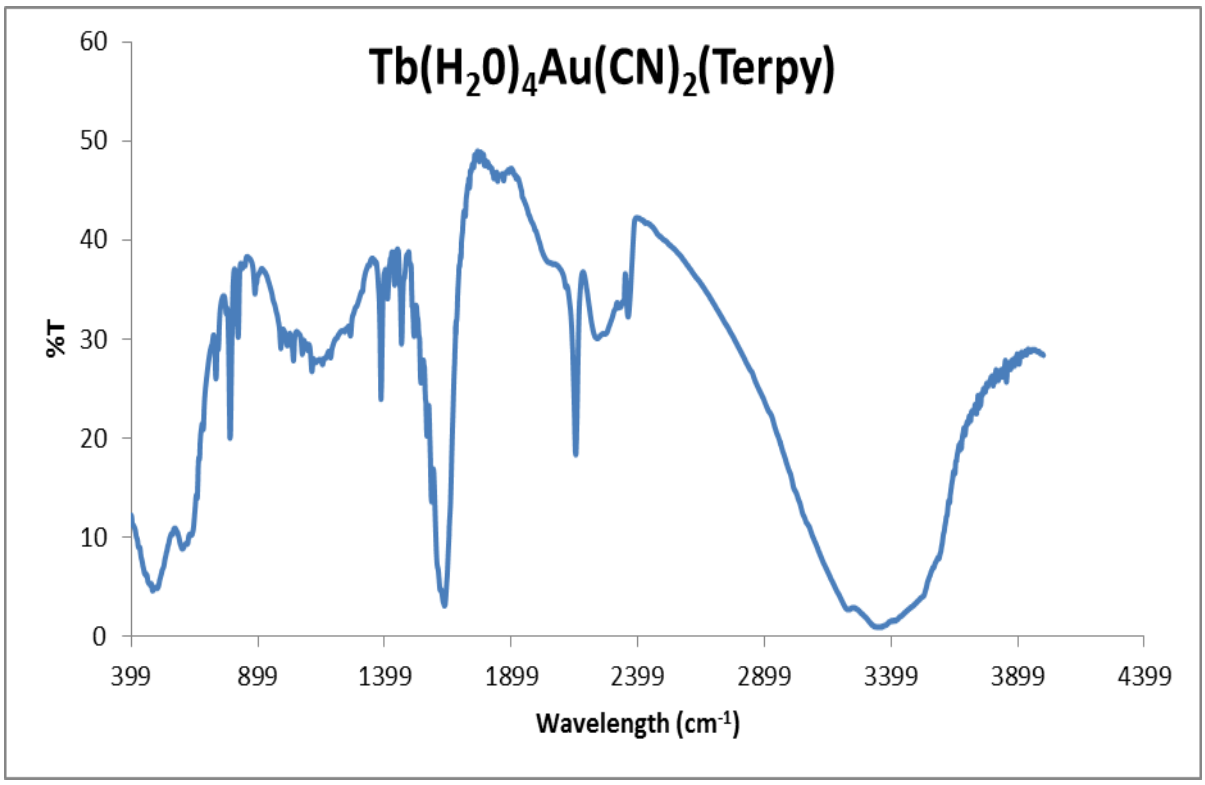

Figure 3.28. Infrared spectrum of compound **3**

3.3.2 Raman studies of 3. The Raman spectrum of compound **3** shows the coordination of CN to the Tb^{3+}. The CN stretching peak of compound **3** is at 2164cm^{-1} shown in Figure 3.29 below.

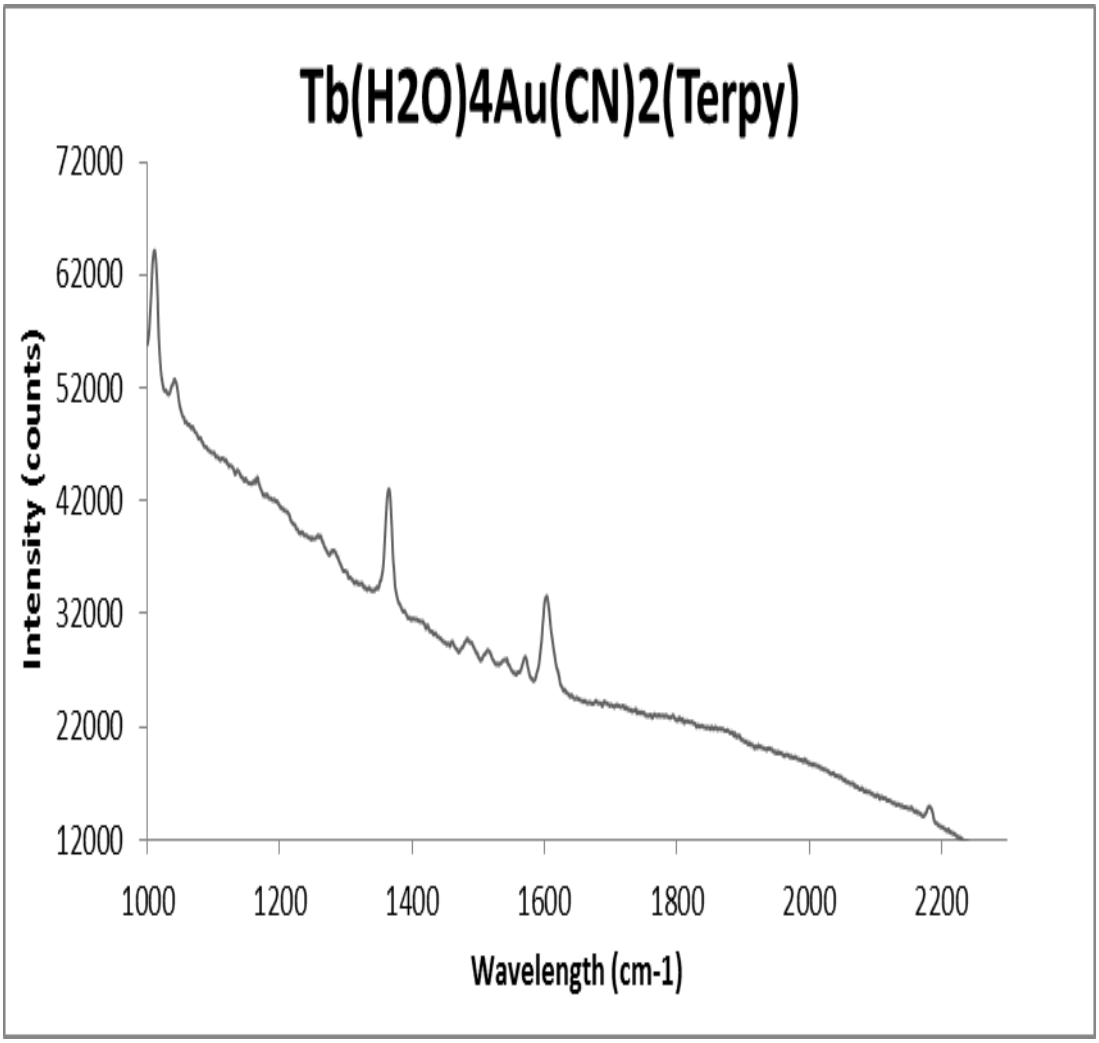

Figure 3.29. Raman spectrum of **3**

3.3.3 Photoluminescence studies of compound 3 The emission spectrum of **3** was collected at room temperature and under liquid nitrogen upon excitation at 343 nm,378 nm and 381 nm is shown in Figure 3.29, 3.30 and 3.31, and 3.32 below. The emission is monitored at 378 nm and 343 nm to determine if there is any energy transfer from $Au(CN)_2^-$ to the lanthanide, Tb^{3+}. The most intense band is around 542 nm when excited at 343 nm and 378 nm, which both peaks corresponds to $^5D_4 \rightarrow {}^7F_5$ transition, which is shown below.

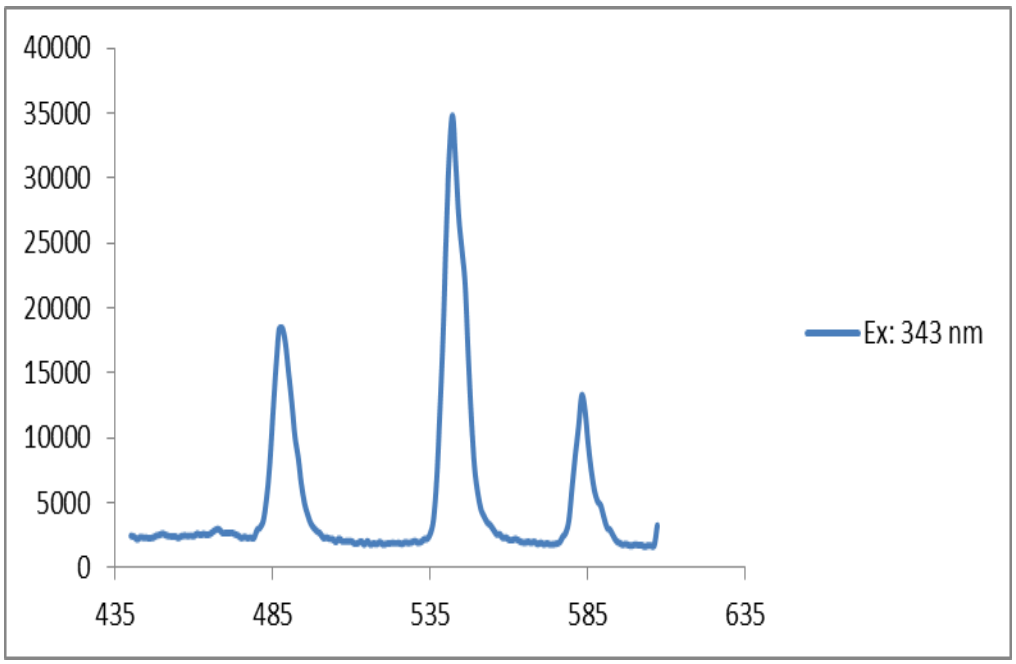

Figure 3.30. Emission spectrum of **3** was collected at room temperature upon excitation at 343nm

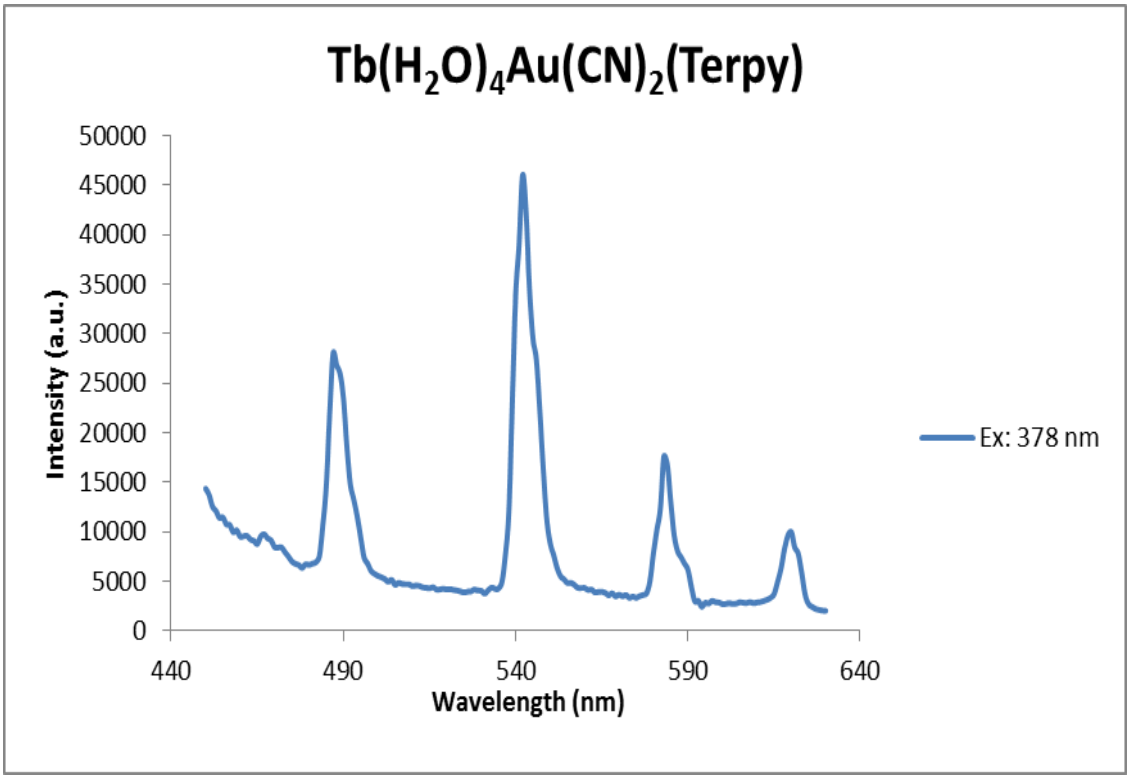

Figure 3.31. Emission spectrum of **3** collected under Liq. N_2 and excited at 378nm

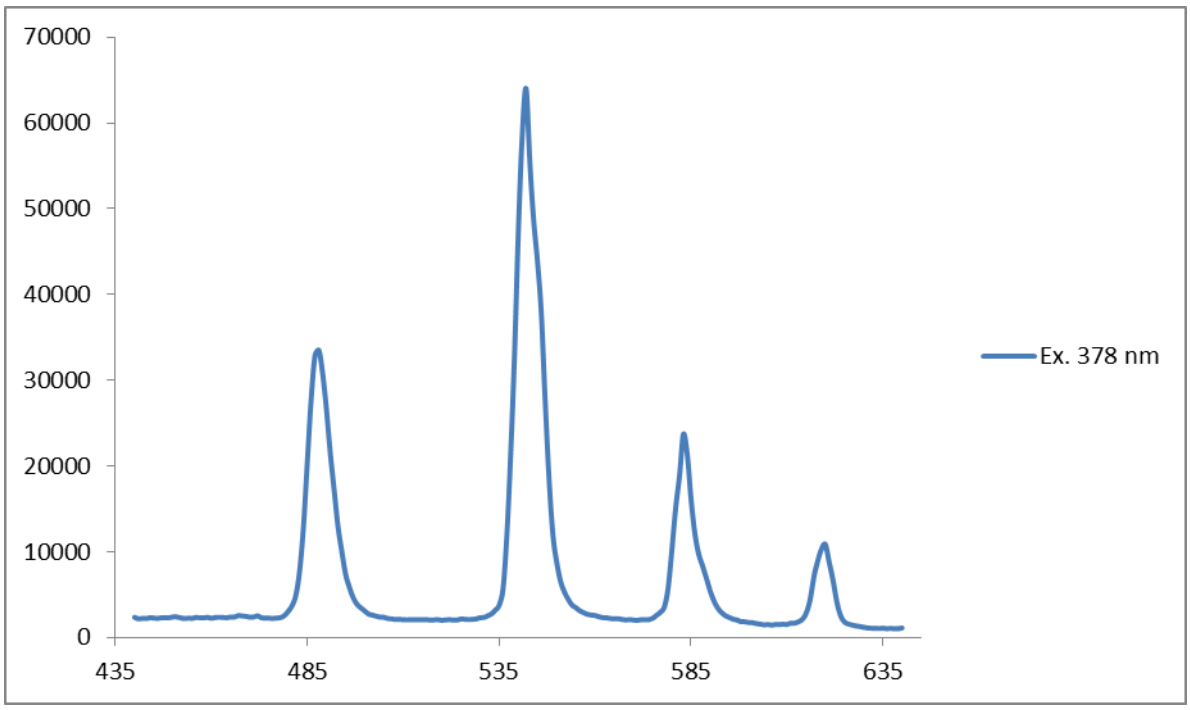

Figure 3.32. Emission spectrum of **3** was collected at room temperature upon excitation at 378nm

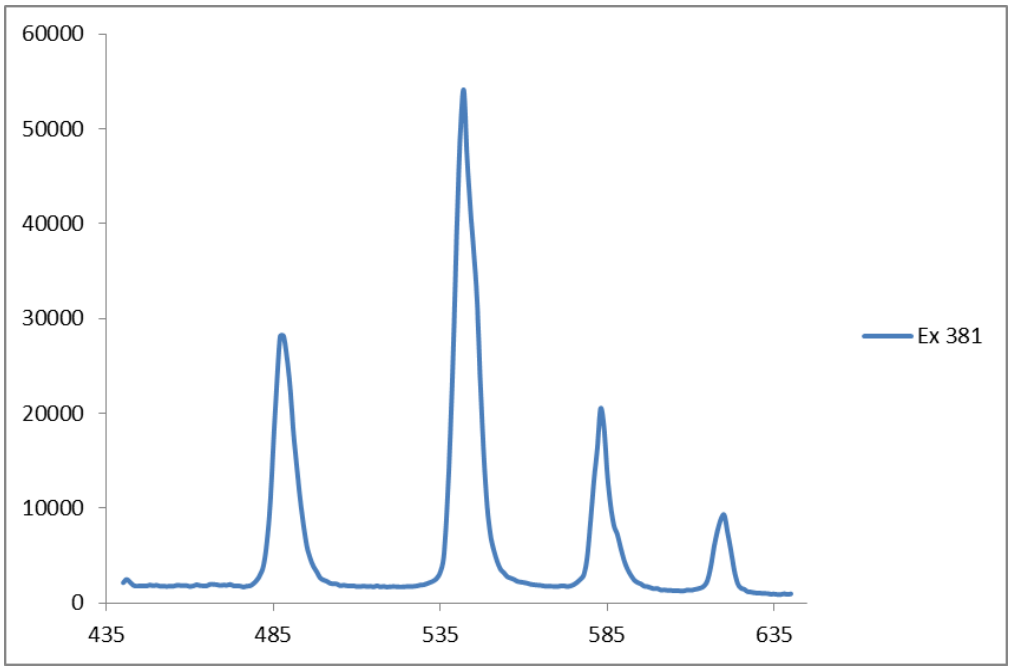

Figure 3.33. Emission spectrum of **3** was collected at room temperature upon excitation at 381nm

The emission spectrum of **3** was also collected when exciting at 385 and 400nm, which is the wavelength for the terpy ligand. In Figures 3.34 and 3.35 the most intense peak is at 542nm, which corresponds to $^5D_4 \rightarrow {}^7F_5$ transition for Tb^{3+}.

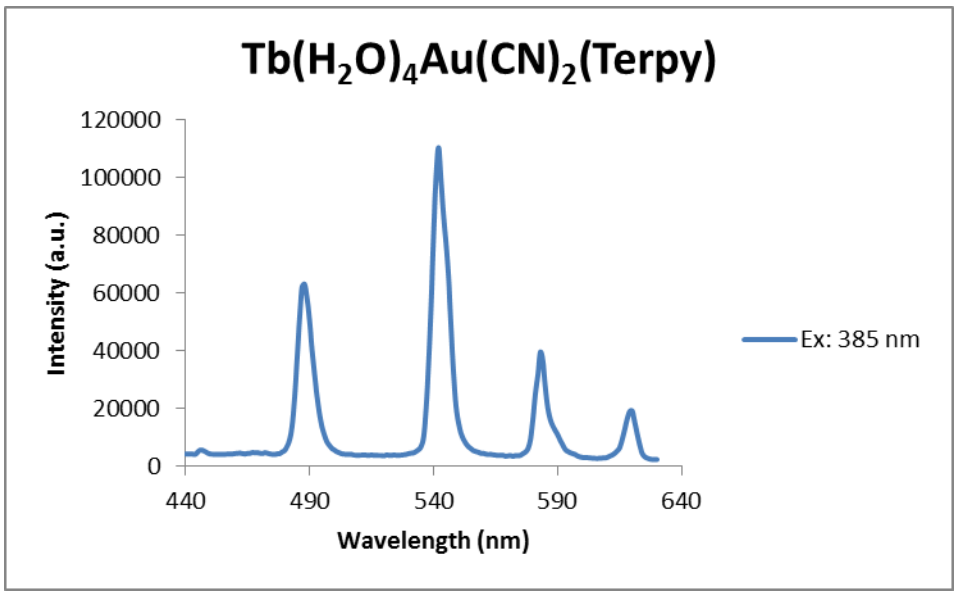

Figure 3.34. Emission spectrum of **3** was collected at room temperature upon excitation at 385nm

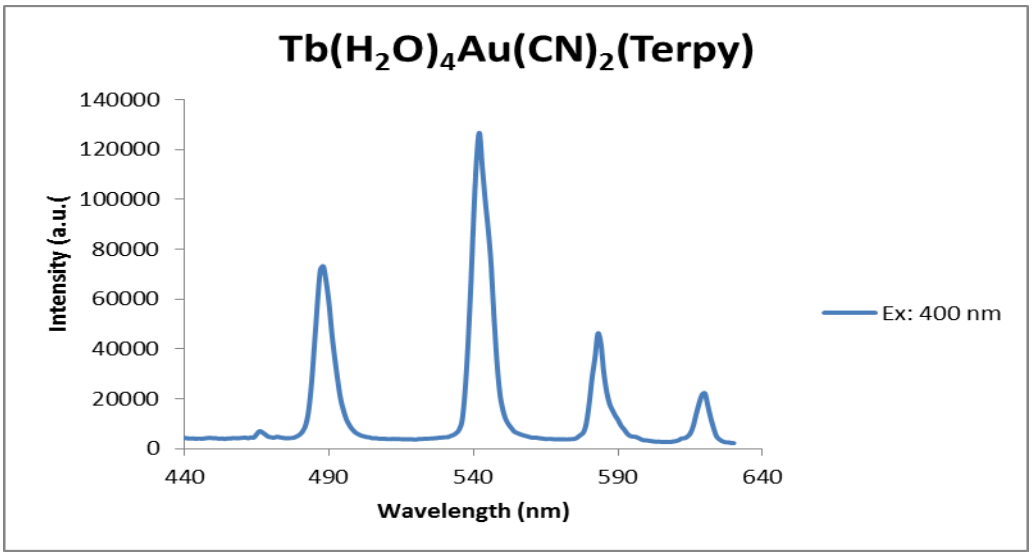

Figure 3.35. Emission spectrum of **3** was collected at room temperature upon excitation at 400nm

Table 3.3

*Emission peak positions assignments for compound **3***

Wavelength (nm)	Wavelength (cm^{-1})	Peak Assignments
487 nm	20533	$^5D_4 \rightarrow {}^7F_6$
542nm	18450	$^5D_4 \rightarrow {}^7F_5$
583nm	17152	$^5D_4 \rightarrow {}^7F_4$
619nm	16155	$^5D_4 \rightarrow {}^7F_3$

Excitation in Figure 3.36 and 3.37 were monitored at 490 nm and 600 nm, which have broad bands at 340 and 375nm respectively. These two bands correspond to the ligand and $KAu(CN)_2$. Excitation spectra of Figure 3.38 and 3.39, and Figure 3.40 were monitored at 541 and 540, and 586 nm.

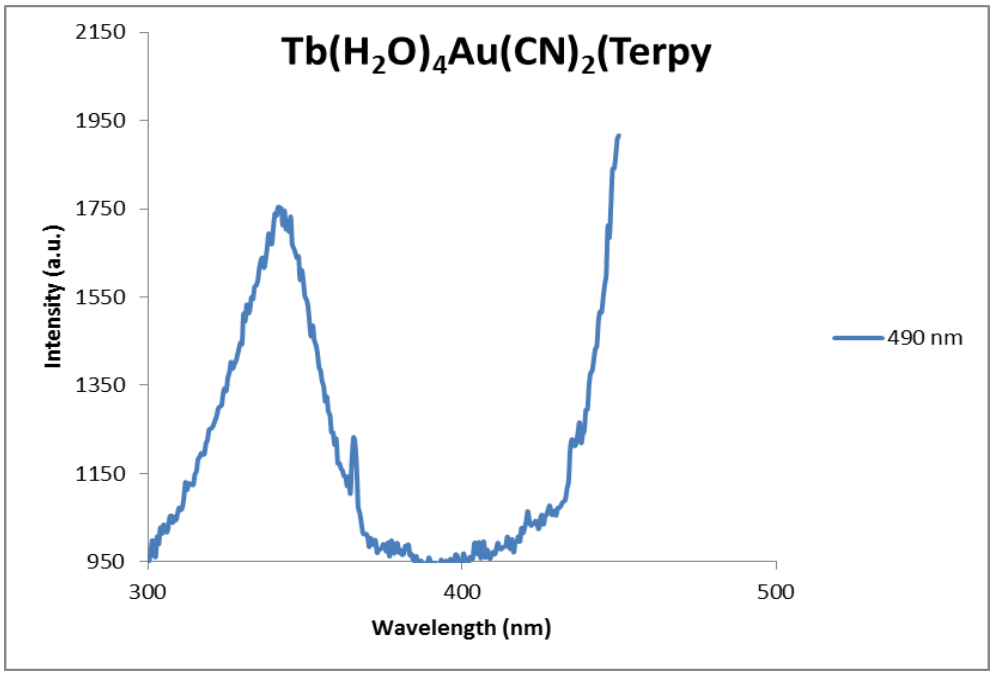

Figure 3.36. Excitation spectrum of **3** when monitored at 490 nm

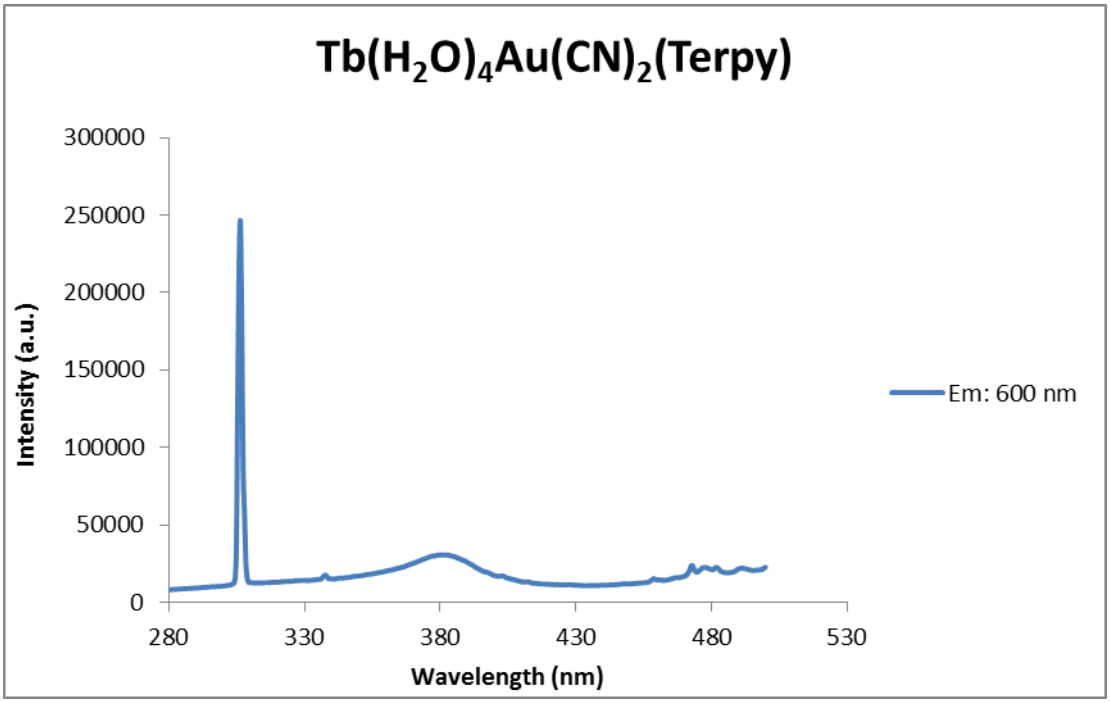

Figure 3.37. Excitation spectra of **3** when monitored at 600 nm

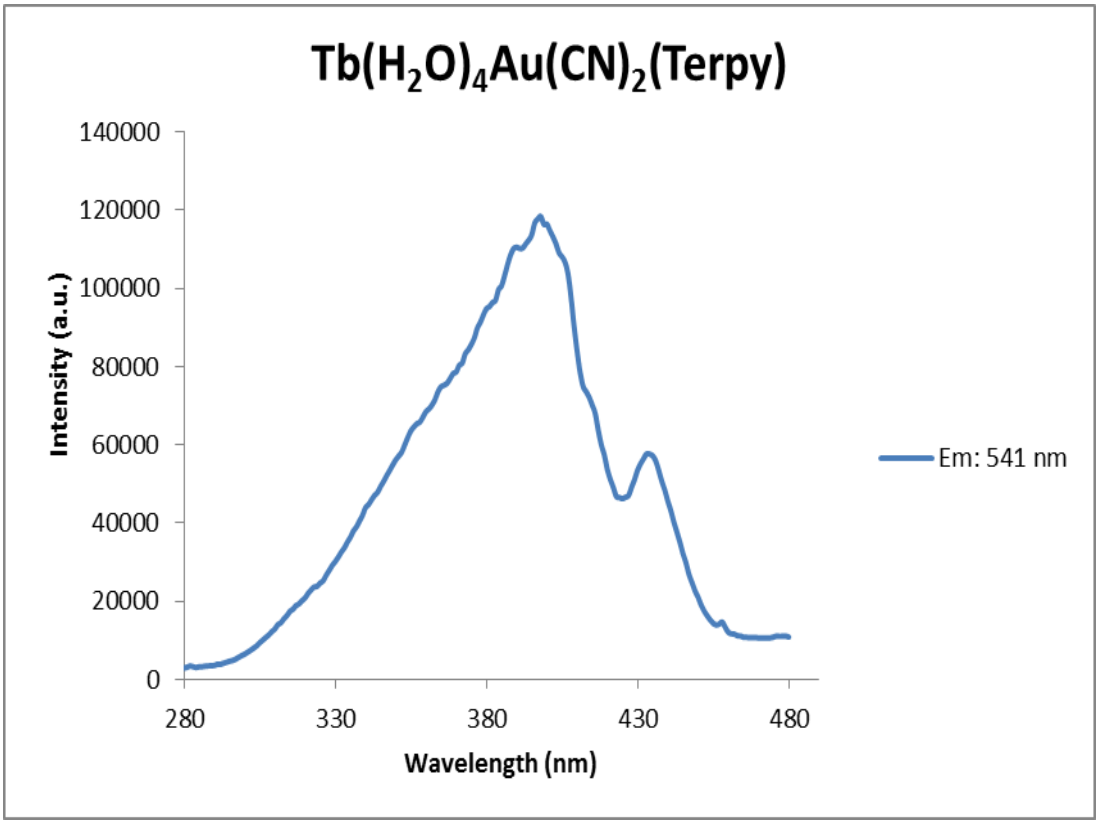

Figure 3.38. Excitation spectrums of **3** when monitored at 541 nm

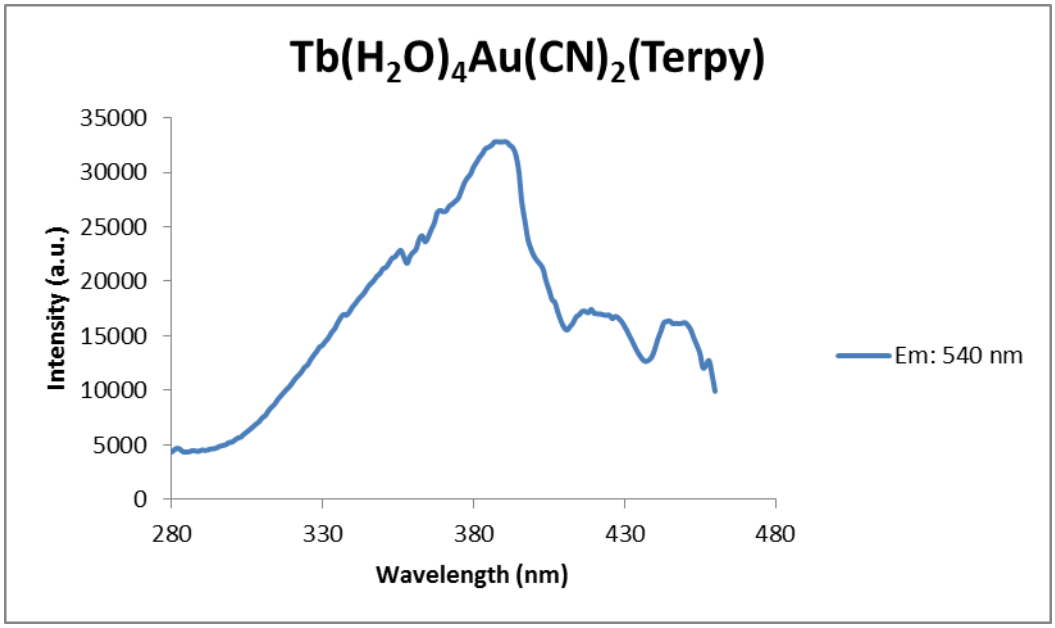

Figure 3.39. Excitation spectrum of **3** collected under Liq. N_2 monitoring at 540 nm

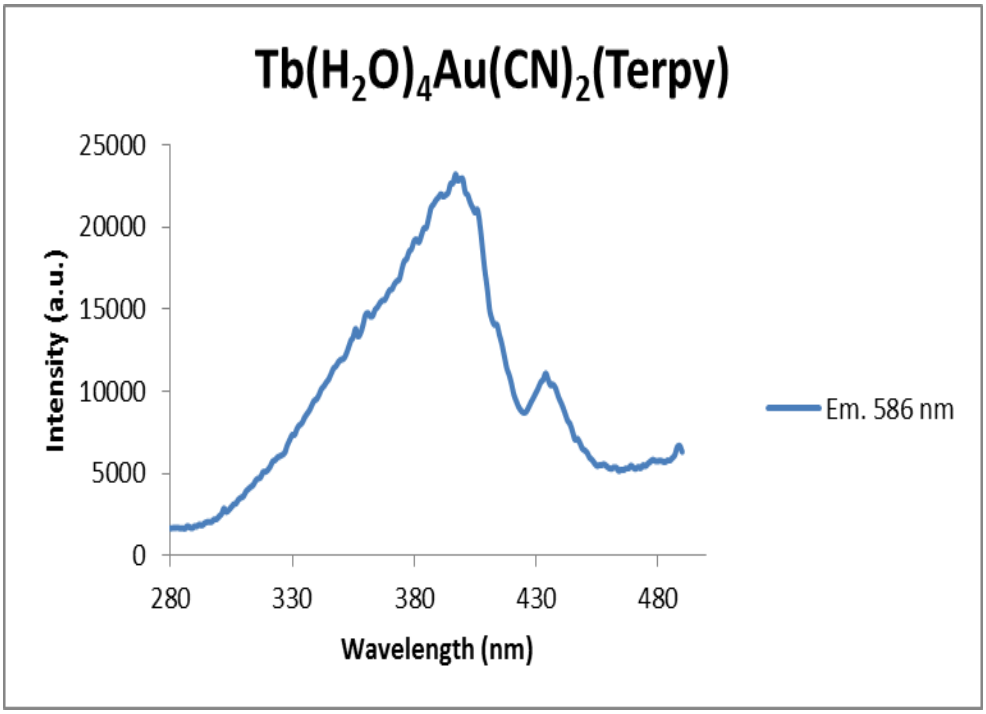

Figure 3.40. Excitation spectrum of **3** when monitored at 586 nm

3.4 Infrared and photoluminescence studies of Compound 4

3.4.1 Infrared studies of 4 Figure 3.41 shows a medium stretch at 2136cm^{-1} which corresponds to the CN stretching from $KAu(CN)_2$. The weak stretching at 3022 cm^{-1} is due to

the ν_{CH} band, which is sp3 hybridized. The broad band around 3342 cm^{-1} is ν_{OH}, which is possible due solvent choice.

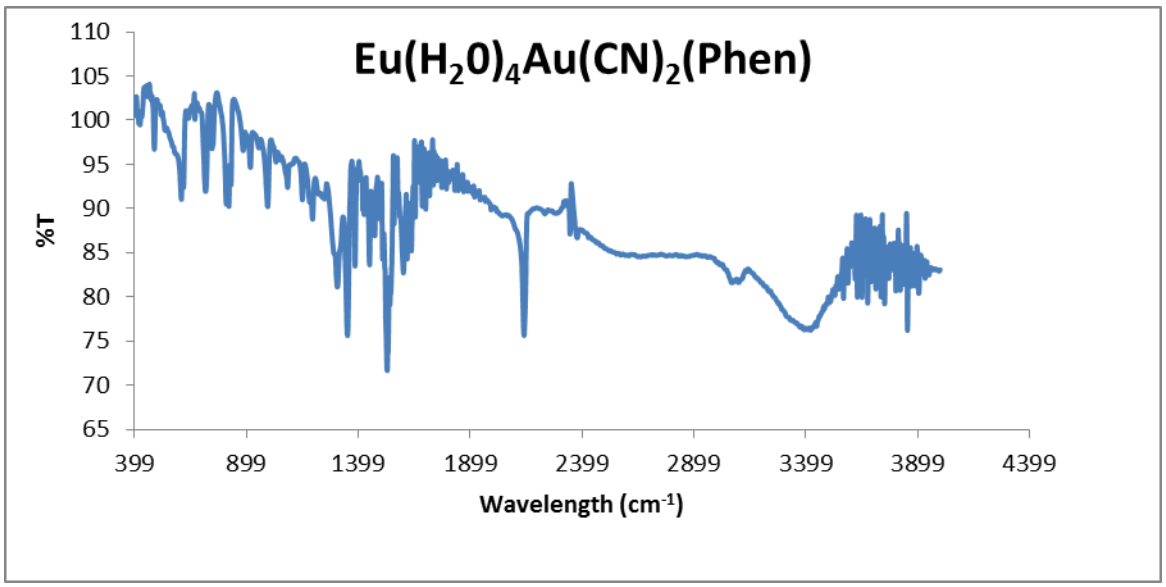

Figure 3.41. Infrared spectrum of **4**

3.4.2 Raman studies of compound 4. Figure 3.42 shows the Raman spectra of Eu^{3+} complex. This shows CN stretching at 2141 cm^{-1}, which indicates that it is Raman active

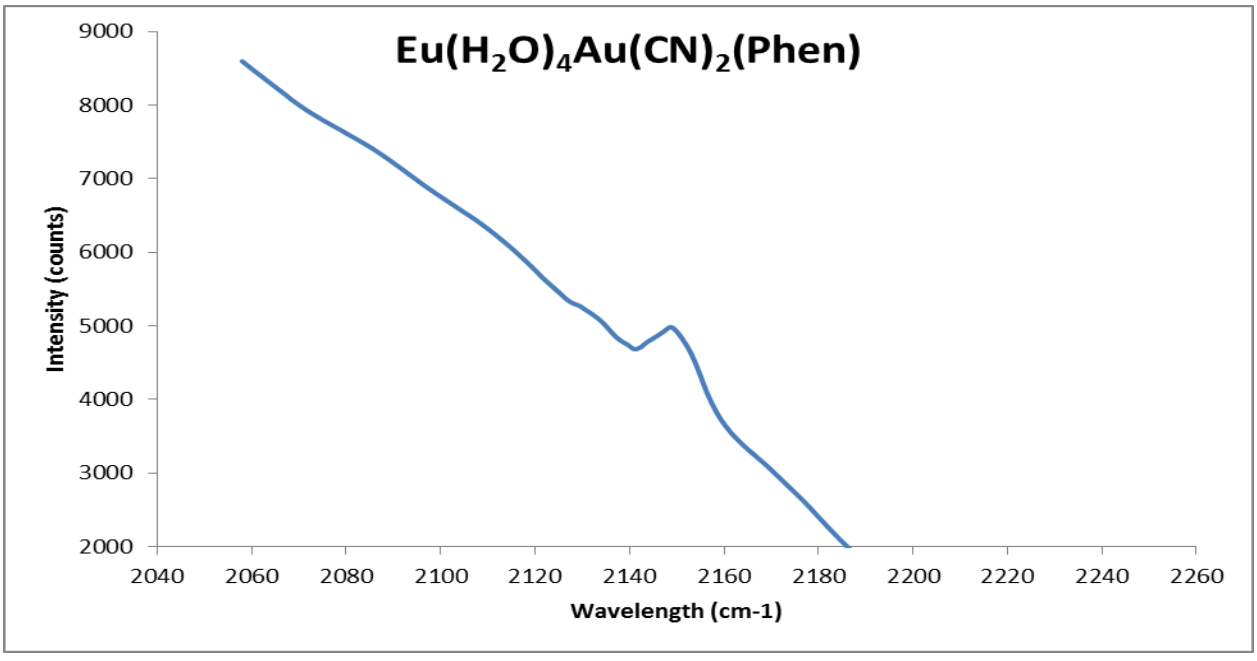

Figure 3.42. Raman spectrum of compound **4**

3.4.3 Photoluminescence studies of compound 4. The emission spectrum of **4** was collected at room upon excitation with 343 nm and 378 nm as shown in Figure 3.43 and 3.45 shown below. When monitored at 343 nm and 378nm the most intense band is around 615nm, which corresponds to $^5D_0 \rightarrow {}^7F_2$. In Figure 3.46 the emission was excited at 343 nm and collected under liquid temperature. When collected under liquid nitrogen the $^5D_0 \rightarrow {}^7F_1$ and $^5D_0 \rightarrow {}^7F_4$ increased significantly. When exciting at 466 nm there are very weak Eu^{3+} bands which is shown in Figure 3.49 below.

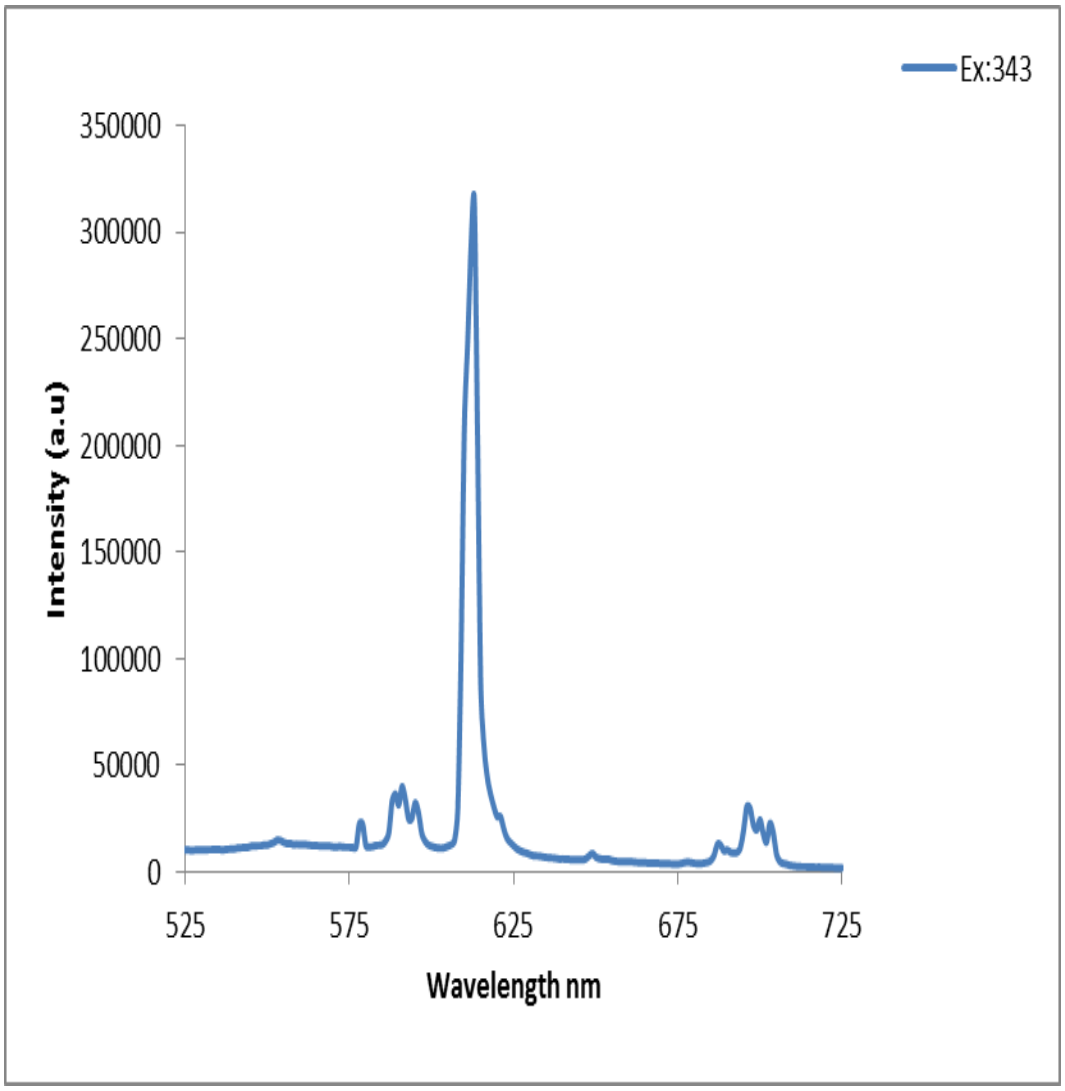

Figure 3.43. Emission spectrum of **4** collected at room temperature upon excitation at 343nm

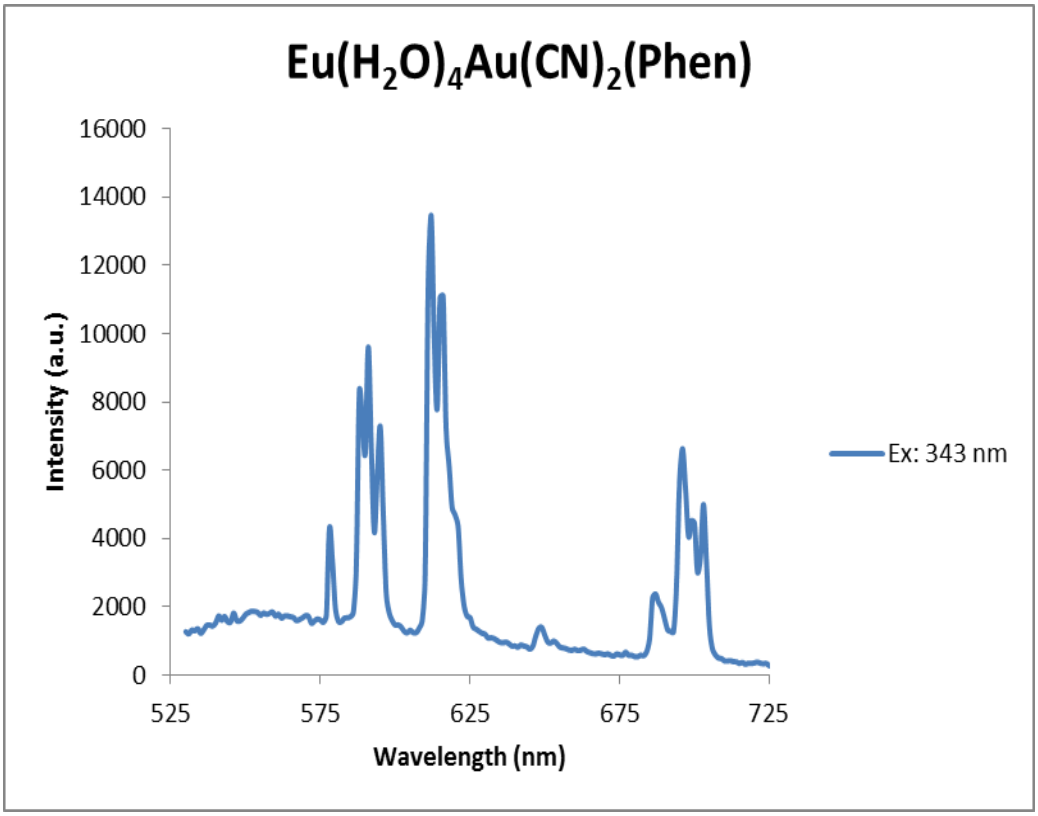

Figure 3.44. Emission spectrum of **4** collected under Liq. N_2 and excited at 343nm

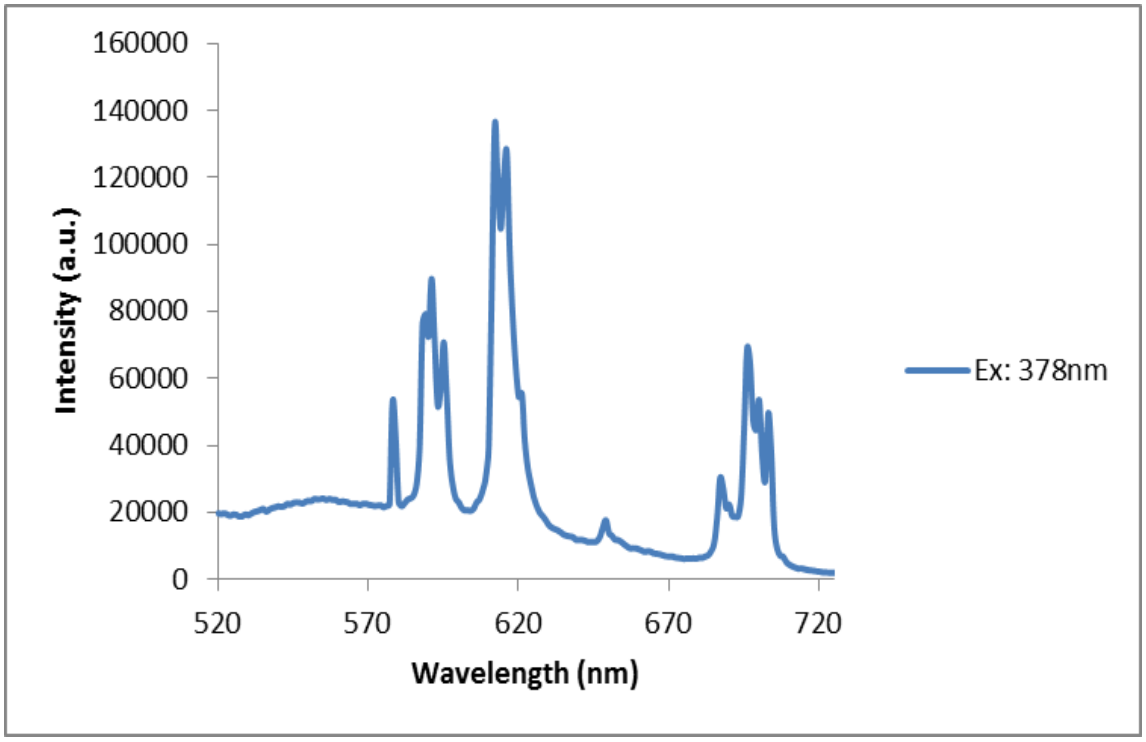

Figure 3.45. Emission spectrum of **4** collected at room temperature upon excitation at 378nm

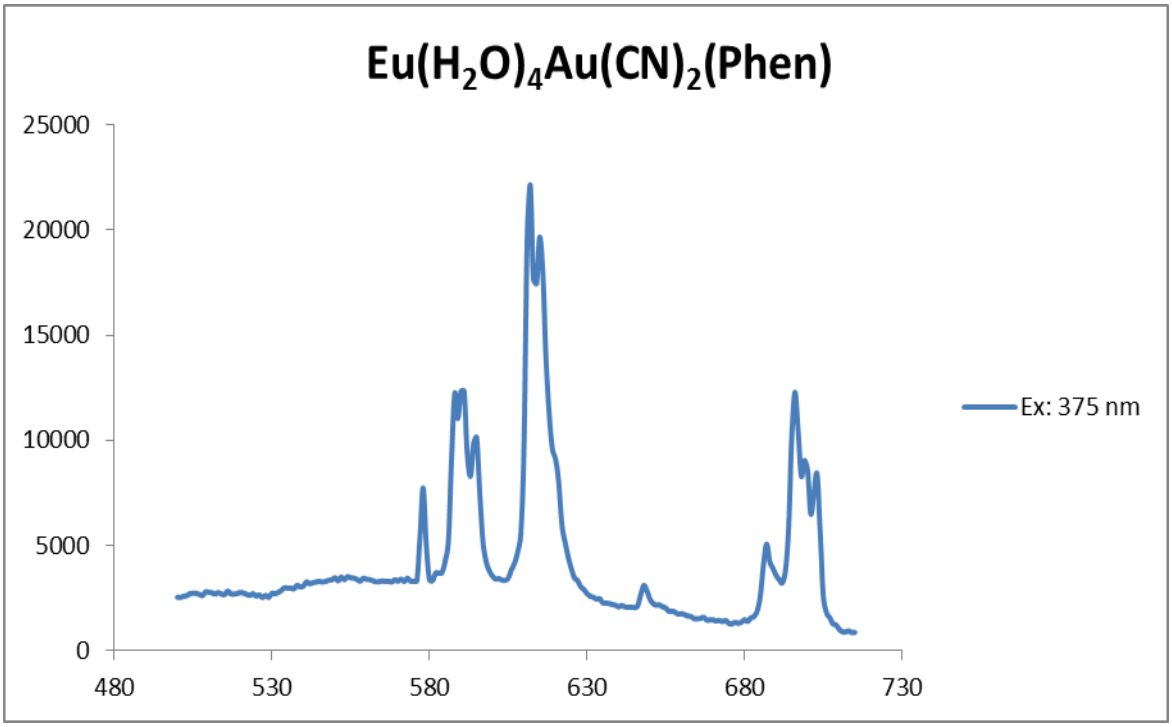

Figure 3.46. Emission Spectra of **4** collected at room temperature when monitored at 375 nm

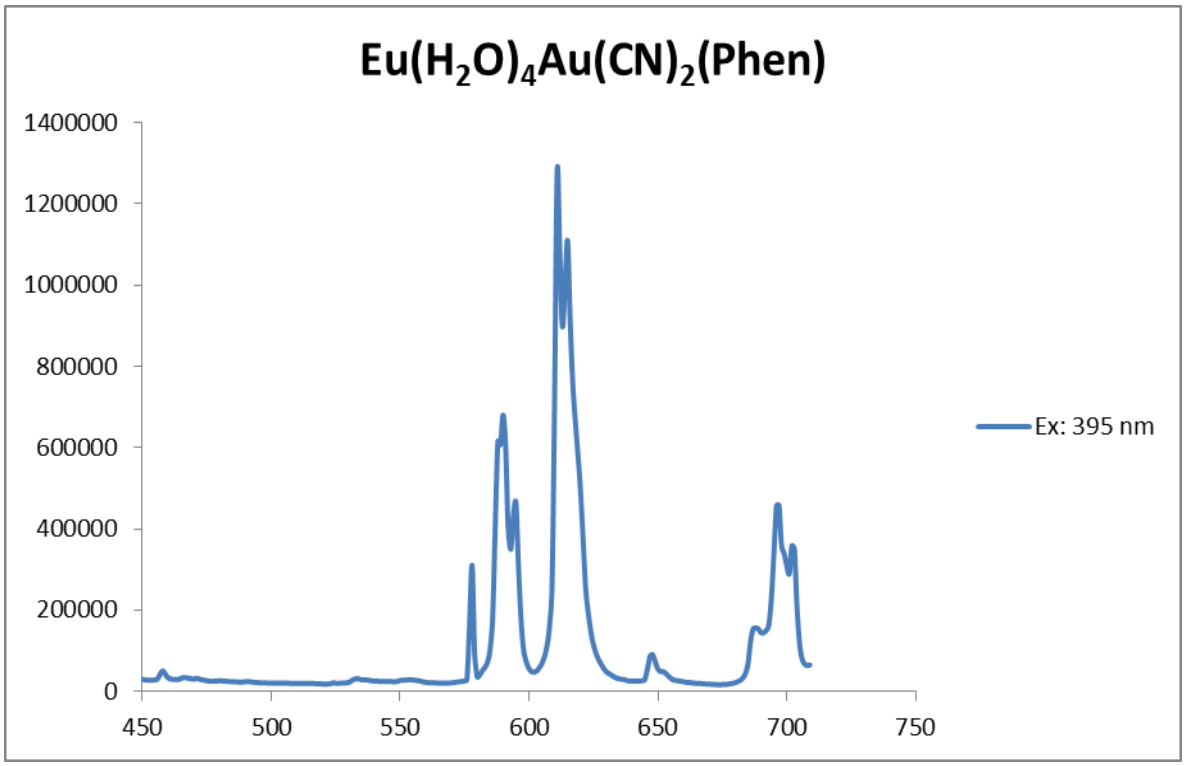

Figure 3.47. Emission spectrum of **4** collected at room temperature when excited at 395 nm

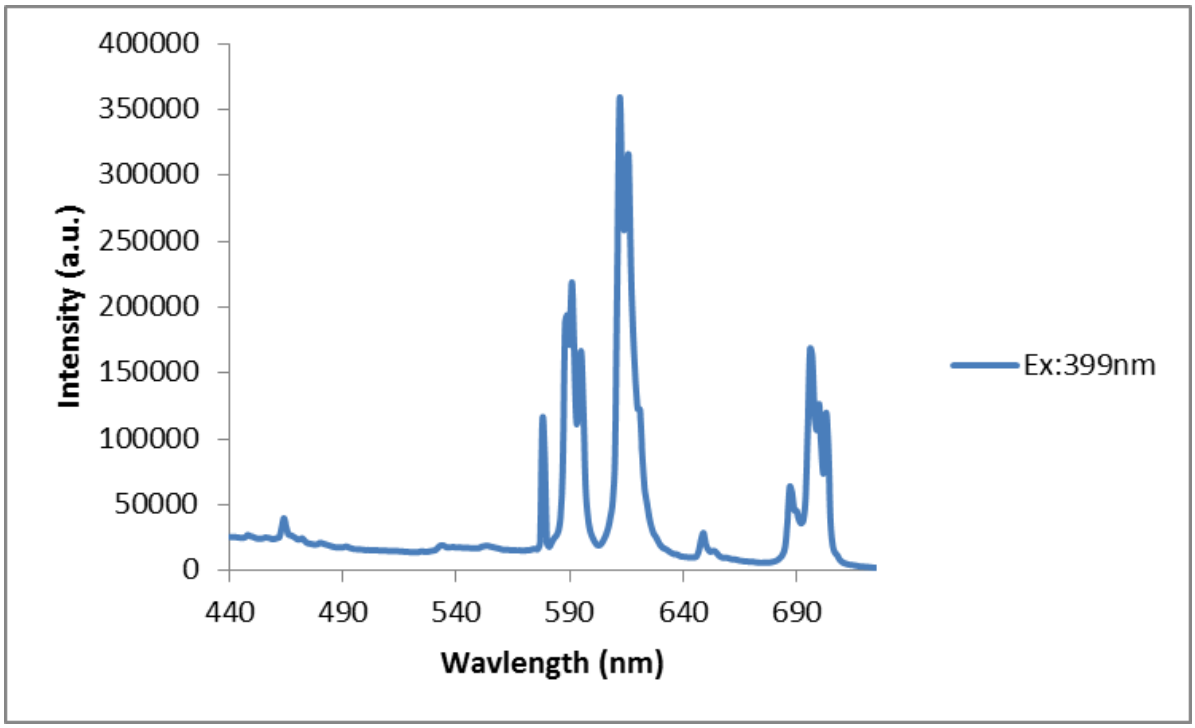

Figure 3.48. Emission spectrum of **4** collected at room temperature upon excitation at 399 nm

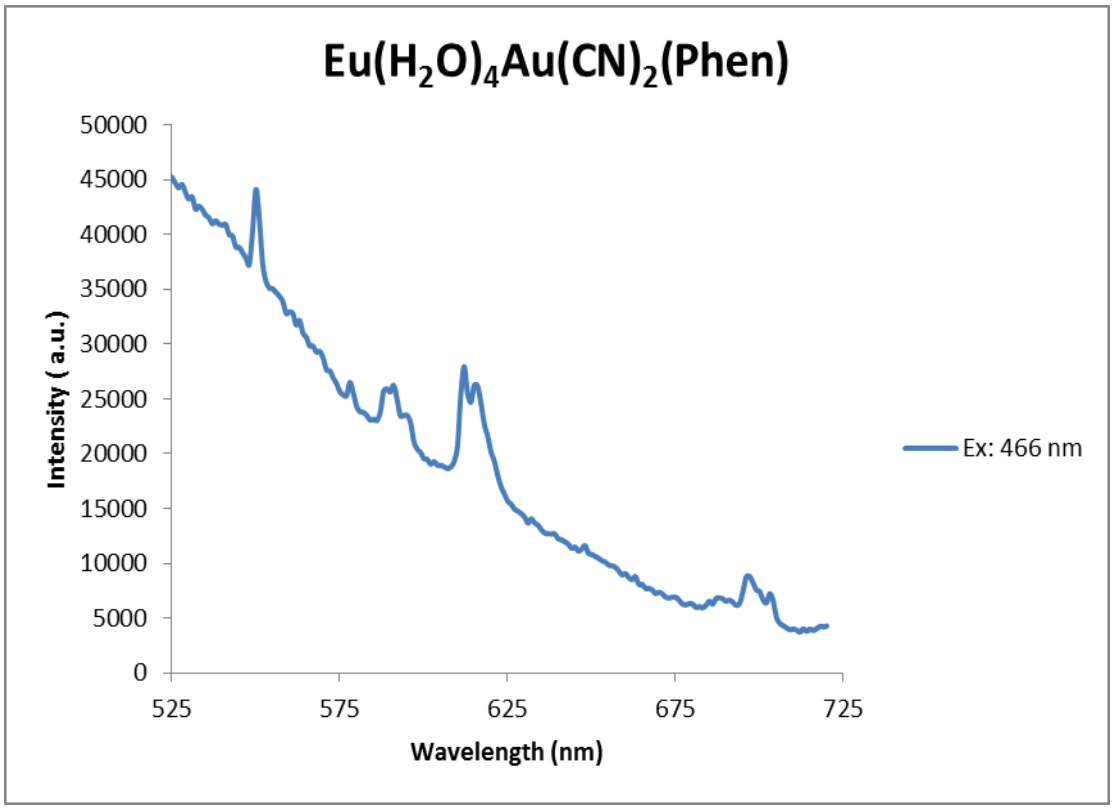

Figure 3.49. Emission spectrum of **4** collected at room temperature upon excitation at 466 nm

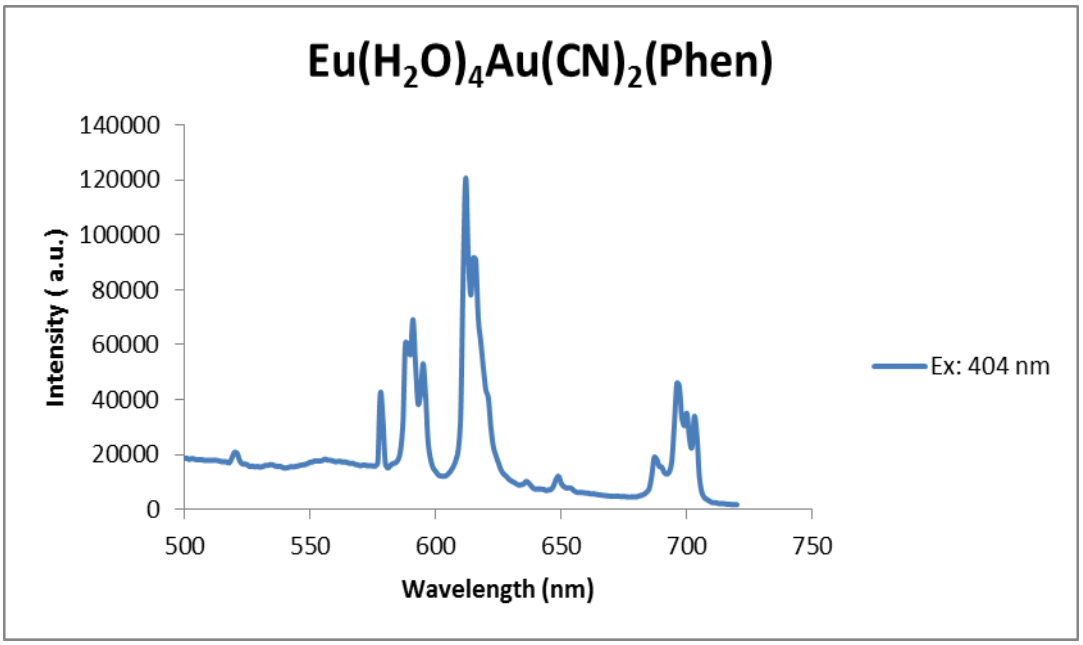

Figure 3.50. Emission spectrum of **4** collected at room temperature upon excitation at 404 nm

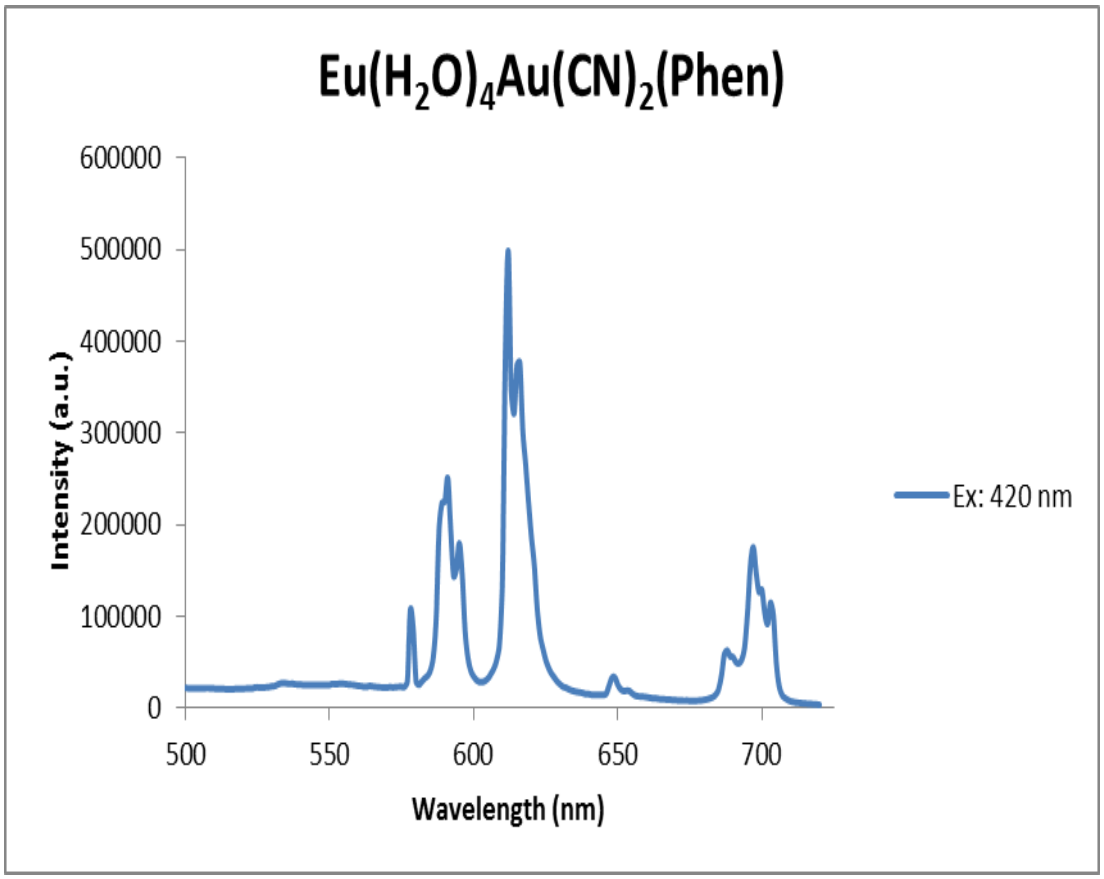

Figure 3.51. Emission spectrum of **4** collected at room temperature when excited at 420 nm

Table 3.4

*Emission peak positions and assignments for compound **4***

Wavelength (nm)	Wavelength (cm^{-1})	Peak Assignments
578 nm	17301	$^5D_0 \rightarrow {}^7F_0$
590nm	16949	$^5D_0 \rightarrow {}^7F_1$
595nm	16806	$^5D_0 \rightarrow {}^7F_1$
615nm	16260	$^5D_0 \rightarrow {}^7F_2$
620nm	16129	$^5D_0 \rightarrow {}^7F_2$
625nm	16000	$^5D_0 \rightarrow {}^7F_2$
649nm	15408	$^5D_0 \rightarrow {}^7F_3$
653nm	15314	$^5D_0 \rightarrow {}^7F_3$
680nm	14706	$^5D_0 \rightarrow {}^7F_4$
690nm	14493	$^5D_0 \rightarrow {}^7F_4$
696nm	14367	$^5D_0 \rightarrow {}^7F_5$
702nm	14245	$^5D_0 \rightarrow {}^7F_5$
710nm	14084	$^5D_0 \rightarrow {}^7F_5$

All excitation spectrums of **4** were collected at room temperature and liquid nitrogen. Figure 3.52 excitation spectrum collected upon emission at 590nm. Figure 3.53 was monitored at 560nm and shows a broad band around 382 nm, and more sharp bands around420-520nm.

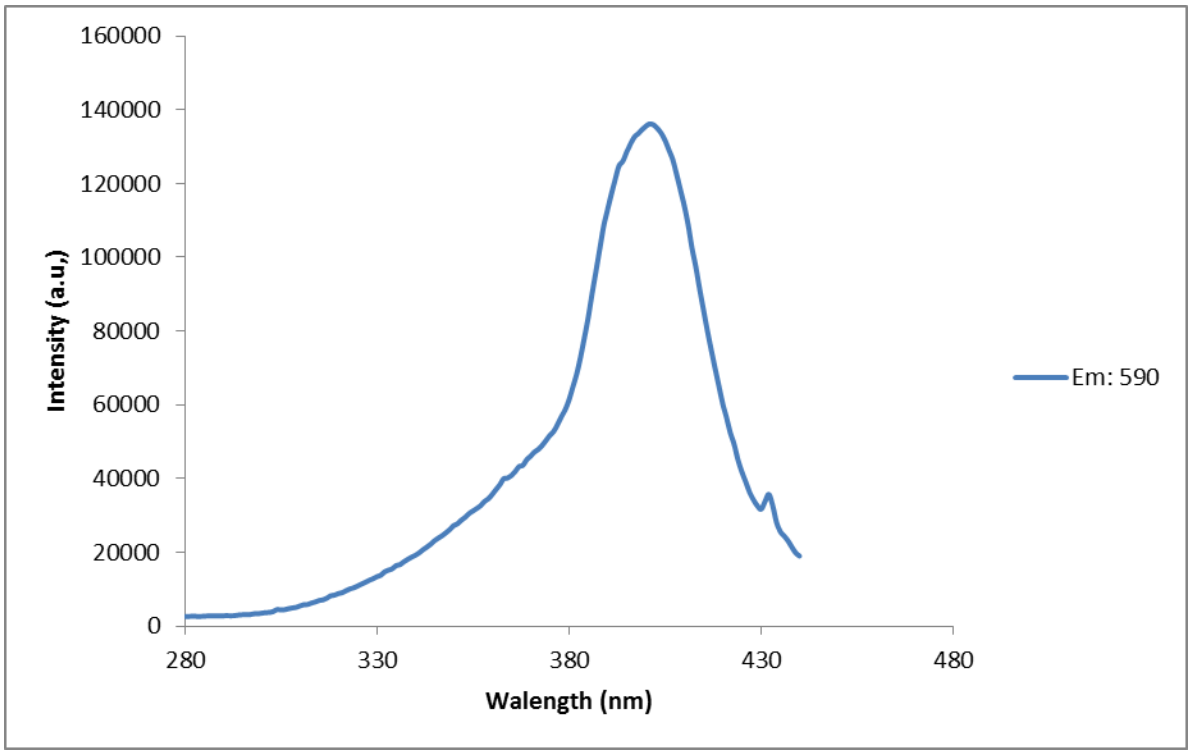

Figure 3.52. Excitation spectrum of **4** collected at room temperature when monitored at 590nm

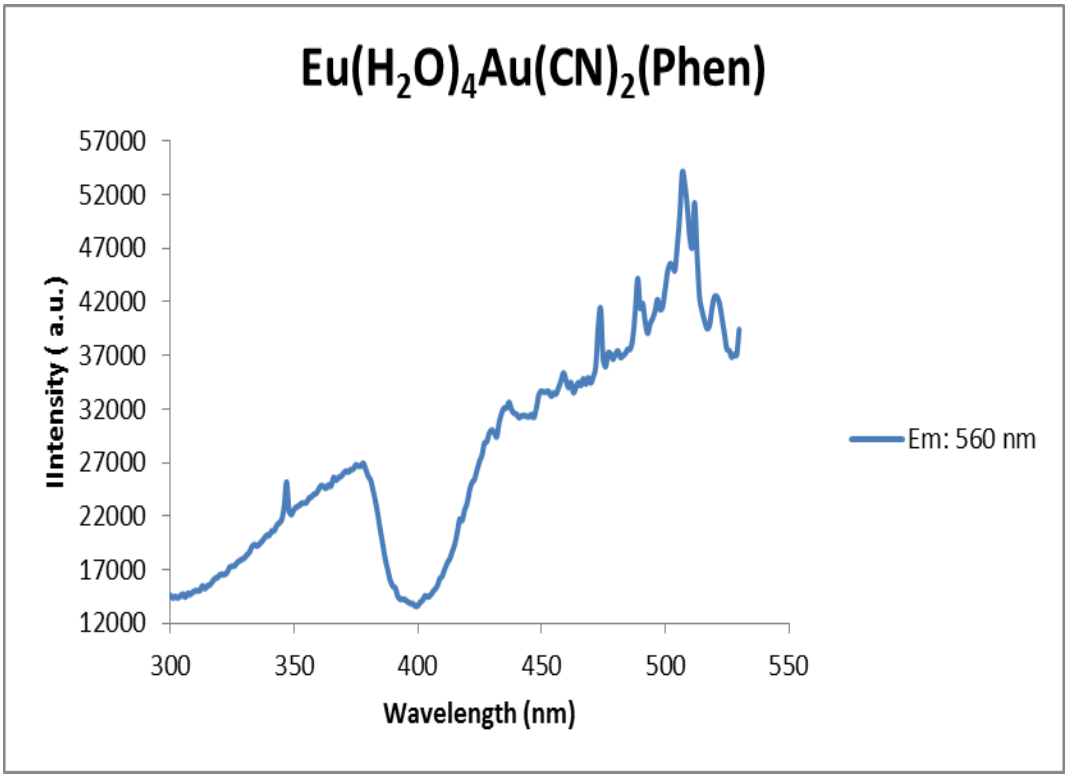

Figure 3.53. Excitation spectra of **4** collected at room temperature when monitored at 560 nm

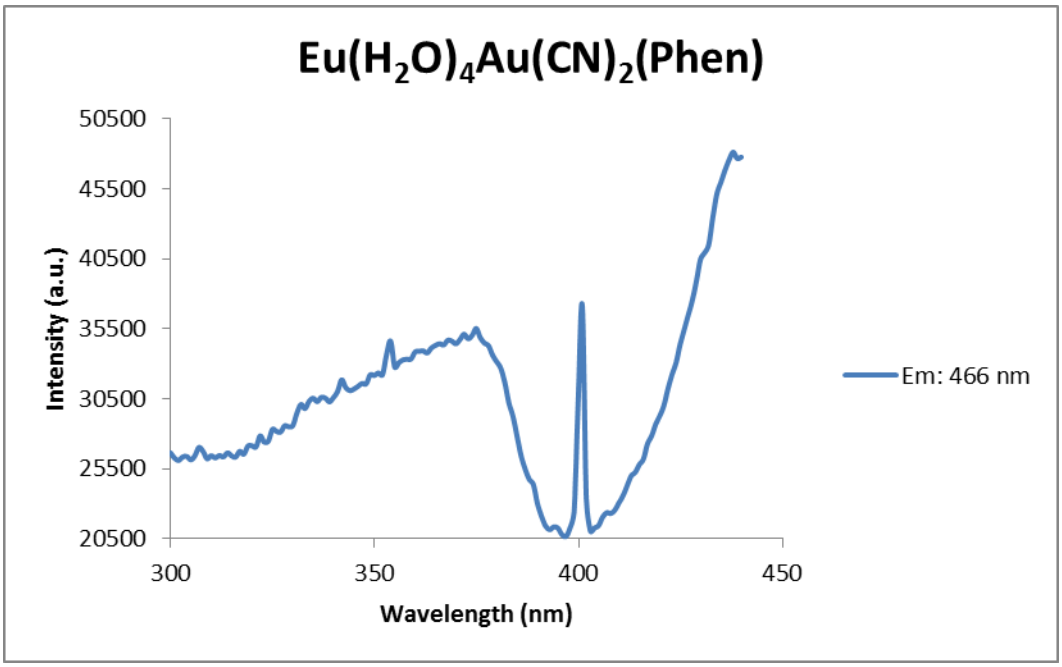

Figure 3.54. Excitation spectra of **4** collected at room temperature when emitted at 466 nm

Excitation spectra shown in Figures 3.55 and 3.56 were collected at room temperature and liquid nitrogen upon emission at 615 nm. Monitoring at 615 nm gives direct excitation of the lanthanide, which gives a broad should at 382 at 398 nm.

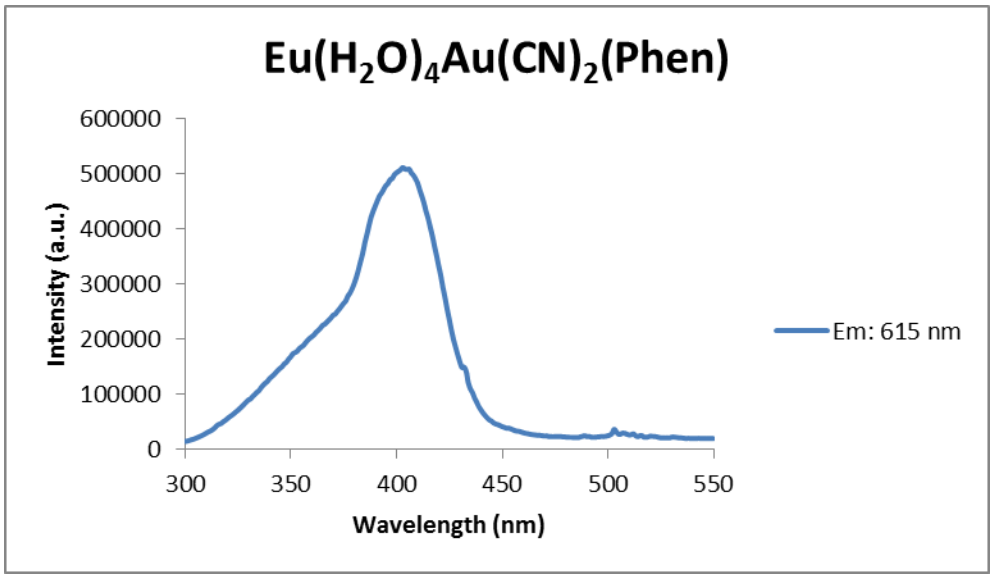

Figure 3.55. Excitation spectra of **4** collected at room temperature when emitted at 615 nm

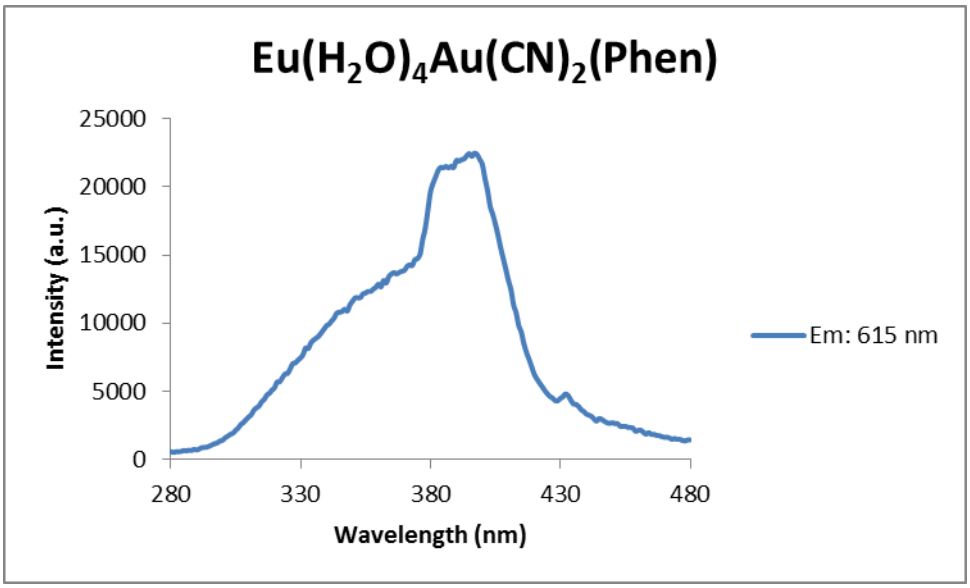

Figure 3.56. Excitation spectrum of **4** collected under Liq. N_2 and monitoring at 615 nm

CHAPTER 4

Discussion

4.1 Vibrational Studies

The IR spectrum of **1** shown in Figure 3.3 has a strong broad band assignable to ν_{OH} at 3327 cm^{-1}. The stretching of the sp^3 hybridized ν_{CH} is observed at 2983 and 3001 cm^{-1}. A medium doublet band is observed at 2146 and 2156 cm^{-1} which corresponds to the ν_{CN} stretching frequency. The Raman studies of **1** also show a more intense singlet ν_{CN} band at 2165 cm^{-1}. Similarly, the IR spectrum of compound **2** shows the ν_{CN} stretching at the same wavenumber as compound **1**, although the Raman data of **2** shows the CN stretching at 2141 cm^{-1}, which is slightly blue shifted when compared to compound **1**. The IR spectra of compound **3** show a CN stretching with values between compounds **1** and **2**. Both the IR and Raman spectra of compound **4** are observed at red shifted positions when compared to the other three compounds. This red shift indicates that electron density increase at the CN bond suggesting that the phen ligand is more pi-donor than the terpy ligand causing weakening of the CN bonds.

4.2 Photoluminescence studies of Tb^{3+} complexes (1 and 3)

Compounds **1** and **3** exhibits uniform bright green luminescence characteristics of Tb^{3+} emission. The excitation spectra of **1** and **3** was collected at room temperature and under liquid nitrogen and monitored at the Tb^{3+} hypersensitive peak at 540 nm and corresponds to $^5D_4 \rightarrow {}^7F_5$ transition. The spectrum shows a broad band at 347 nm assignable to the $\pi-\pi*$ transitions corresponding to the terpy ligand. Another broad band is also observed at 384nm assignable to the charge transfer transition within the $Au(CN)_2^-$ system. The weak and sharp peaks at 403 and 413 nm are assignable to f-f transition within the Tb^{3+}ion. The dominant broad bands, which are centered at 347 nm and 384 nm, are uncharacteristic of f-f transitions. Observation of

characteristic Tb^{3+} emission lines upon excitation into these broad bands unambiguously demonstrates that the sensitized emission is achieved through antenna effect of terpyridine-based π-π* intraligand triplet states and Au-based triplet transitions. The emission spectra of compounds **1** and **3** were also collected at room temperature and under liquid nitrogen. The complexes have sharp bands at 487, 540, 579, and 615 nm attributable to $^5D_4 \rightarrow {}^7F_{6,\,5,\,4,\,3}$ transitions of Tb^{3+}, respectively.

Comparison of the emission intensities at the broad bands (347 and 384 nm) and at the f-f direct excitation lines indicates that the sensitized emission is significantly dominant indicating that the ligand-centered and the charge transitions are the principal route for the delivery of excited energy into the terbium's $4f^n$ electronic levels.

4.3 Photoluminescence Studies of Eu^{3+} Complexes (2 and 4)

The excitation spectra of compounds **2** and **4** were collected by monitoring at the 615 nm emission line. Both compounds show a broad band at ~370 nm, indicating a π–π^* transitions within the phen and terpy ligands. The excitation spectra of both compounds also contain sharp f-f transition at longer wavelengths. The dominance of the broad band uncharacteristic of f-f transition within the Eu3+ electronic levels clearly indicates that ligand and CT transfer
The emission spectra of compound **2** and **4** show all the characteristics of Eu^{3+}. The emission spectra of compounds **2** and **4** both show $^5D_0 \rightarrow {}^7F_0$ transition which is an f-f forbidden transition. Even though $^5D_0 \rightarrow {}^7F_0$ transition is forbidden it may gain intensity through J mixing due the crystal field effect under low symmetry. The point symmetry of the $^5D_0 \rightarrow {}^7F_0$ transition should have both magnetic dipole allowed and electric dipole allowed transitions. All spectra of compound **4** show the maximum number of splitting (three) for the $^5D_0 \rightarrow {}^7F_1$ transition, which indicates that the europium ion occupies low site symmetry. In contrast, compound **2** splits into

a doublet suggesting that higher site symmetry occupation. When exciting both Eu^{3+} complexes at 378 nm, the intensity ratio of the hypersensitive $^5D_0 \rightarrow {}^7F_2$ transition to the magnetic dipole $^5D_0 \rightarrow {}^7F_1$ transition is 1.22 for compound **2** and 1.88 for compound **4** suggesting the dominance of electric dipole transition in this system. The phen ligand has a greater electric dipole effect than the terpy ligand on the Eu^{3+} environment. When the compounds are monitored under liquid nitrogen temperature there is an increase in intensity of the electric dipole $^5D_0 \rightarrow {}^7F_1$ transition. Compound **2** shows five well-defined lines for the $^5D_0 \rightarrow {}^7F_4$ which is partially allowed by magnetic dipole contribution, whereas for compound **4** there are four well-defined lines indicating a point symmetry of c_2v. When compound **4** is excited at 343 and 378 nm excited state energy transfer from the phen and the $Au(CN)_2^-$ to the lanthanide is clearly evident. The sensitized emission intensity is significantly higher than the direct f-f excitation as can be observed in the intensity differences of the 343 nm vs. the 466 nm excitations, respectively. Finally the dominance of the electric diploe transition in these systems clearly indicates that the Eu^{3+} ion occupies a non centrosymmetric site occupation.

CHAPTER 5

Conclusion

This work shows four new compounds that have been successfully synthesized and characterized. Detail vibrational and photoluminescence studies including IR and Raman spectroscopy were conducted in these microcrystalline powdered products. This research has shown that both the ligand and transition metal complex coordinated the lanthanide center can sensitize the emission and resulting in significant emission enhancement. The new complexes that were studied are $[Tb(H_2O)_2(Au(CN)_2)(C_{22}H_{17}N_3)(TPAO)]Cl_3$ **1**, $[Eu(H_2O)_5(Au(CN)_2)(C_{22}H_{17}N_3)]Cl_3$ **2**, $[Tb(H_2O)_4(Au(CN)_2)(C_{22}H_{17}N_3)]Cl_3$ **3**, and $[Eu(H_2O)_3Au(CN)_2(Phen)]Cl_3$**,4.** Each one of these complexes shows a dual donor intramolecular energy transfer, both from the ligand and from $Au(CN)_2^-$.

References

1. Harvey, E. N., *A history of luminescence from the earliest times until 1900*. American Philosophical Society: Philadelphia, 1957.
2. Valeur, B.; Berberan-Santos, M. r. N., A Brief History of Fluorescence and Phosphorescence before the Emergence of Quantum Theory. *J. Chem. Educ.* **2011,** *88* (6), 731-738.
3. (a) Weber, M. J., Multiphonon Relaxation of Rare-Earth Ions in Yttrium Orthoaluminate. *Physical Review B* **1973,** *8* (1), 54-64; (b) Weber, M. J.; Varitimos, T. E.; Matsinger, B. H., Optical Intensities of Rare-Earth Ions in Yttrium Orthoaluminate. *Physical Review B* **1973,** *8* (1), 47-53.
4. Wiberg, E. W. N. H. A. F., *Inorg. chem.*. Academic Press; De Gruyter: San Diego; Berlin; New York, 2001.
5. *Shriver & Atkins inorganic chemistry*. 4th ed. ed.; Oxford University Press ; Oxford ; 2006.
6. Clegg, R. M., Fluorescence resonance energy transfer. *Curr. Opin. Biotechnol.* **1995,** *6* (1), 103-110.
7. Werts, M. H., Making sense of lanthanide luminescence. *Sci. Prog.* **2005,** *88* (2), 101-131.
8. Cotton, S., *Lanthanide and Actinide Chemistry*. Wiley: 2007.
9. Bünzli, J.-C. G.; Comby, S.; Chauvin, A.-S.; Vandevyver, C. D. B., New Opportunities for Lanthanide Luminescence. *Journal of Rare Earths* **2007,** *25* (3), 257-274.

10. Elbanowski, M.; Mąkowska, B., The lanthanides as luminescent probes in investigations of biochemical systems. *Journal of Photochemistry and Photobiology A: Chemistry* **1996,** *99* (2–3), 85-92.

11. Choppin, G. R.; Peterman, D. R., Applications of lanthanide luminescence spectroscopy to solution studies of coordination chemistry. *Coord. Chem. Reviews* **1998,** *174* (1), 283-299.

12. (a) Colis, J. C. F.; Staples, R.; Tripp, C.; Labrecque, D.; Patterson, H., Metallophilic Interactions in Closed-Shell d10 Metal−Metal Dicyanide Bonded Luminescent Systems Eu[AgxAu1-x(CN)2]3 and Their Tunability for Excited State Energy Transfer. *J. Phys. Chem. B* **2004,** *109* (1), 102-109; (b) Kłonkowski, A. M.; Lis, S.; Pietraszkiewicz, M.; Hnatejko, Z.; Czarnobaj, K.; Elbanowski, M., Luminescence Properties of Materials with Eu(III) Complexes: Role of Ligand, Coligand, Anion, and Matrix. *Chemistry of Materials* **2003,** *15* (3), 656-663; (c) Assefa, Z.; Haire, R. G.; Raison, P. E., Photoluminescence and Raman studies of Sm^{3+} and Nd^{3+} ions in zirconia matrices: example of energy transfer and host–guest interactions. *Spectrochimica Acta Part A: Molecular and Biomolecular Spectroscopy* **2004,** *60* (1–2), 89-95.

13. Bünzli, J.-C. G.; Piguet, C., Taking advantage of luminescent lanthanide ions. *Chem. Soc. Rev.* **2005,** *34* (12), 1048-1077.

14. (a) Haas, Y.; Stein, G., Pathways of radiative and radiationless transitions in europium(III) solutions. The role of high energy vibrations. *J. Phys. Chem.* **1971,** *75* (24), 3677-3681; (b) Horrocks, W. D.; Sudnick, D. R., Lanthanide ion probes of structure in biology. Laser-induced luminescence decay constants provide a direct measure of the number of metal-coordinated water molecules. *J. Am. Chem. Soc.* **1979,** *101* (2), 334-340.

15. Tong, B.-H.; Wang, S.-J.; Jiao, J.; Ling, F.-R.; Meng, Y.-Z.; Wang, B., Novel luminescent lanthanide complexes covalently linked to a terpyridine-functionalized silica network. *Journal of Photochemistry and Photobiology A: Chemistry* **2007,** *191* (1), 74-79.

16. Taydakov, I. V.; Zaitsev, B. E.; Krasnoselskiy, S. S.; Starikova, Z. A., Synthesis, X-ray structure and luminescent properties of Sm3+ ternary complex with novel heterocyclic β-diketone and 1,10-phenanthroline (Phen). *J. of Rare Earths* **2011,** *29* (8), 719-722.

17. Schubert, U. S.; Winter, A.; Newkome, G. R., *Terpyridine-based materials: for catalytic, optoelectronic and life science applications*. John Wiley & Sons: 2011.

18. Bencini, A.; Lippolis, V., 1, 10-Phenanthroline: a versatile building block for the construction of ligands for various purposes. *Coord. Chem. Rev.* **2010,** *254* (17), 2096-2180.

19. Chelucci, G.; Addis, D.; Baldino, S., A new approach to the 1, 10-phenanthroline core. *Tetrahedron Lett.* **2007,** *48* (19), 3359-3362.

20. Whitehead, K.; Assefa, Z., Synthesis, characterization, and photoluminescence properties of europium(III) and phosphine oxides. **2009**.